



HAL
open science

A re-evaluation of the Plenus Cold Event, and the links between CO₂, temperature, and seawater chemistry during OAE 2

Lauren O'Connor, Hugh C Jenkyns, Stuart Robinson, Serginio R.C. Remmelzwaal, Sietske Batenburg, Ian Parkinson, Andy Gale

► To cite this version:

Lauren O'Connor, Hugh C Jenkyns, Stuart Robinson, Serginio R.C. Remmelzwaal, Sietske Batenburg, et al.. A re-evaluation of the Plenus Cold Event, and the links between CO₂, temperature, and seawater chemistry during OAE 2. *Paleoceanography and Paleoclimatology*, 2020, 35 (4), pp.e2019PA003631. 10.1029/2019PA003631 . insu-02406694

HAL Id: insu-02406694

<https://insu.hal.science/insu-02406694>

Submitted on 17 Feb 2021

HAL is a multi-disciplinary open access archive for the deposit and dissemination of scientific research documents, whether they are published or not. The documents may come from teaching and research institutions in France or abroad, or from public or private research centers.

L'archive ouverte pluridisciplinaire **HAL**, est destinée au dépôt et à la diffusion de documents scientifiques de niveau recherche, publiés ou non, émanant des établissements d'enseignement et de recherche français ou étrangers, des laboratoires publics ou privés.

Paleoceanography and Paleoclimatology

RESEARCH ARTICLE

10.1029/2019PA003631

Key Points:

- This study is the first to review mechanistic interactions, and temporal leads and lags, between temperature, seawater chemistry, and CO₂ within the Plenus interval
- The negative carbon-isotope excursion during the Plenus interval was a global event driven by a CO₂ increase, and appears decoupled from cooling and circulation changes
- Cooling was not globally synchronous; local climatic and environmental responses to the CO₂ change are more complex than previously understood

Supporting Information:

- Supporting Information S1

Correspondence to:

L. K. O'Connor,
lko@arizona.edu

Citation:

O'Connor, L. K., Jenkyns, H. C., Robinson, S. A., Remmelzwaal, S. R. C., Batenburg, S. J., Parkinson, I. J., & Gale, A. S. (2020). A re-evaluation of the Plenus cold event, and the links between CO₂, temperature, and seawater chemistry during OAE 2. *Paleoceanography and Paleoclimatology*, 35, e2019PA003631. <https://doi.org/10.1029/2019PA003631>

Received 17 APR 2019

Accepted 26 NOV 2019

Accepted article online 4 DEC 2019

A Re-evaluation of the Plenus Cold Event, and the Links Between CO₂, Temperature, and Seawater Chemistry During OAE 2

Lauren K. O'Connor^{1,2}, Hugh C. Jenkyns¹, Stuart A. Robinson¹, Serginio R. C. Remmelzwaal³, Sietske J. Batenburg^{1,4}, Ian J. Parkinson³, and Andy S. Gale⁵

¹Department of Earth Sciences, University of Oxford, Oxford, UK, ²Department of Geosciences, University of Arizona, Tucson, AZ, USA, ³School of Earth Sciences, University of Bristol, Bristol, UK, ⁴Université de Rennes, CNRS, Géosciences Rennes, Rennes, France, ⁵School of Earth and Environmental Sciences, University of Portsmouth, Portsmouth, UK

Abstract The greenhouse world of the mid-Cretaceous (~94 Ma) was punctuated by an episode of abrupt climatic upheaval: Oceanic Anoxic Event 2. High-resolution climate records reveal considerable changes in temperature, carbon cycling, and ocean chemistry during this climatic perturbation. In particular, an interval of cooling has been detected in the English Chalk on the basis of an invasive boreal fauna and bulk oxygen-isotope excursions registered during the early stages of Oceanic Anoxic Event 2—a phenomenon known as the Plenus Cold Event, which has tentatively been correlated with climatic shifts worldwide. Here we present new high-resolution neodymium-, carbon-, and oxygen-isotope data, as well as elemental chromium concentrations and cerium anomalies, from the English Chalk exposed at Dover, UK, which we evaluate in the context of >400 records from across the globe. A negative carbon-isotope excursion that correlates with the original “Plenus Cold Event” is consistently expressed worldwide, and CO₂ proxy records, where available, indicate a rise and subsequent fall in CO₂ over the Plenus interval. However, variability in the timing and expression of cooling at different sites suggests that, although sea-surface paleotemperatures may reflect a response to global CO₂ change, local processes likely played a dominant role at many sites. Variability in the timing and expression of changes in water mass character, and problems in determining the driver of observed proxy changes, suggest that no single simple mechanism can link the carbon cycle to oceanography during the Plenus interval and other factors including upwelling and circulation patterns were locally important. As such, it is proposed that the Plenus carbon-isotope event is a more reliable stratigraphic marker to identify the Plenus interval, rather than any climatic shifts that may have been overprinted by local effects.

1. Introduction to Oceanic Anoxic Event 2 and the Plenus Cold Event

At a global scale, the latest Cenomanian–earliest Turonian interval was characterized by the most significant environmental perturbation of the Late Cretaceous: Oceanic Anoxic Event 2 (OAE 2; Schlanger & Jenkyns, 1976; Arthur et al., 1990; Jenkyns, 2010). OAE 2 was an interval of extreme greenhouse conditions, with high temperatures and high atmospheric pCO₂ (Arthur et al., 1988; Jarvis et al., 2011; Jenkyns et al., 1994; Kuypers et al., 1999). The leading hypothesis for the initiation of the OAE invokes the submarine emplacement of large igneous provinces releasing vast quantities of CO₂ into the ocean and atmosphere, leading to an intensified greenhouse climate that caused an accelerated hydrological cycle and enhanced nutrient flux to the oceans (e.g., Jenkyns, 2003). Volcanism and/or other types of basalt–seawater interaction may also have supplied biologically significant metals directly into seawater (Du Vivier et al., 2014; Jenkyns et al., 2017; Orth et al., 1993; Snow et al., 2005; Turgeon & Creaser, 2008). Nutrient input is credited with enhancing organic productivity on a global scale, increasing the carbon flux to the sea floor to form the characteristic black-shale record and a distinctive positive δ¹³C excursion—together constituting the hallmark of the OAE—as well as progressively leading to significant regional deoxygenation in many parts of the world ocean, particularly the North Atlantic (e.g., Jenkyns, 2010; Pearce et al., 2009). Bottom-water anoxia and hypoxia possibly affected 40–50% of the global ocean, but with euxinic (sulfidic) bottom waters affecting a much smaller percentage (Dickson et al., 2016, 2017; Monteiro et al., 2012; Ostrander et al., 2017; Owens et al., 2013).

Accelerated burial rates of planktonic organic matter, whose biosynthesis led to preferred incorporation of the lighter ¹²C isotope, resulted in a marked positive carbon-isotope excursion recorded in different

sedimentary archives around the world (e.g., Bowman & Bralower, 2005; Jarvis et al., 2011; Jenkyns et al., 1994; Schlanger et al., 1987; Scholle & Arthur, 1980; Tsikos et al., 2004; Voigt et al., 2006; Wendler, 2013). The canonical model suggests that, eventually, increased rates of organic-carbon burial would have caused a drawdown of atmospheric CO₂, ultimately triggering global cooling that led to a weakening of the factors promoting carbon burial (Arthur et al., 1988; Gale et al., 2019; Jenkyns et al., 1994; Kuypers et al., 1999; Sinninghe Damsté et al., 2010; van Bentum et al., 2012).

Lithium- and calcium-isotope records suggest that, in addition to organic-carbon burial, enhanced silicate weathering in both subaerial (under conditions of an accelerated hydrological cycle) and submarine environments during the OAE may have aided in the drawdown of CO₂ and the termination of the OAE (Blättler et al., 2011; van Bentum et al., 2012; Pogge von Strandmann et al., 2013; Jenkyns et al., 2017; Jenkyns, 2018). However, it has recently been argued that the persistence of high temperatures globally throughout the latter stages of OAE 2 and into the early Turonian suggests that CO₂ did not decline, and that some other mechanism was responsible for the termination of the event, rather than a cessation of climatic factors favorable for “black shale” formation (Robinson et al., 2019).

While the sedimentary expression of the OAE 2 interval varies worldwide, the carbon-isotope evolution of OAE 2 is broadly similar in all investigated sites across the world where the stratigraphic record is tolerably complete (Figure 1): first buildup, trough, second buildup, plateau with spikes, followed by decay toward background (Paul et al., 1999; Tsikos et al., 2004; Wendler, 2013).

In the early stages of OAE 2, between peaks “a” and “b” (Figure 1), a brief (~40 kyr; Jarvis et al., 2011) interval of cooling occurred that was first recognized in the chalk of the Anglo-Paris Basin by the southerly incursion of boreal fauna (notably the belemnite *Praeactinocamax plenus*) into the paleo-European midlatitudes (Jefferies, 1962, 1963). This interval was later discovered to be coeval with a positive oxygen-isotope excursion, and it was found that the spread of boreal fauna extended southward into the Tethys (southern France; Gale & Christensen, 1996). This period of cooling was termed the “Plenus Cold Event” (PCE) after the Plenus Marls, a relatively clay-rich interval in the English Chalk where the fall in temperature is registered (Figure 1; Jenkyns et al., 2017). Cooling during OAE 2 has been identified from a number of sea-surface temperatures (SST) proxies from marine sections across the Northern Hemisphere (e.g., Desmares et al., 2016; Forster et al., 2007; Gale et al., 2019; Jarvis et al., 2011; Sinninghe Damsté et al., 2010; van Helmond et al., 2016), suggesting that the entire North Atlantic Ocean and its surrounding epicontinental seas were affected. Broadly synchronous with the PCE, a period of extensive bottom-water re-oxygenation occurred throughout the Western Interior Seaway of North America and the North Atlantic (Eicher & Diner, 1985; Eicher & Worstell, 1970; Eldrett et al., 2014; Forster et al., 2007; Friedrich et al., 2006; Keller et al., 2008; Keller & Pardo, 2004; Leckie, 1985; Zhou et al., 2015). The strata affected by re-oxygenation have been referred to as pertaining to the “Benthic Oxidic Zone,” although this event is typically equated with the Plenus Cold Event (e.g., Eldrett et al., 2014; Jenkyns et al., 2017; van Helmond et al., 2016), suggesting a global forcing mechanism for both climatic and redox changes.

Many authors have attributed the PCE to a decline in atmospheric $p\text{CO}_2$ (e.g., Barclay et al., 2010; Gale et al., 2019; Jarvis et al., 2011; Sinninghe Damsté et al., 2010), suggesting that the transient negative $\delta^{13}\text{C}$ excursion signifies reduced global burial of organic carbon under more oxygenated conditions, recorded at sites around the world (Erbacher et al., 2005; Hasegawa et al., 2013; Jarvis et al., 2011; Voigt et al., 2008). Estimates of the magnitude of the atmospheric $p\text{CO}_2$ decrease during OAE 2 range from 20–25% (Freeman & Hayes, 1992; Jarvis et al., 2011) to 40–80% (Kuypers et al., 1999). Ongoing volcanism and/or basalt–seawater interaction during the early part of OAE 2 and the resultant input of greenhouse gases to the atmosphere is thought to have counterbalanced the carbon drawdown, maintaining relatively high temperatures except during the onset of the PCE, ultimately allowing the return to greenhouse conditions only when the rate of carbon dioxide supply exceeded the rate of its sequestration (Jenkyns et al., 2017). While a causal relationship has been postulated between carbon-cycle dynamics and cooling during the Plenus interval (e.g., Forster et al., 2007; Jarvis et al., 2011; Kuypers et al., 1999; Sinninghe Damsté et al., 2010), the existing records are from widespread locations and, as such, explanations of the PCE are sensitive to the stratigraphic correlation between sites. Understanding the timing of paleoenvironmental changes, both local and global, is therefore critical for disentangling the driver of climate change during this perturbation of the carbon cycle. As such, we seek here to investigate the synchronicity of environmental changes at the location where the PCE was first

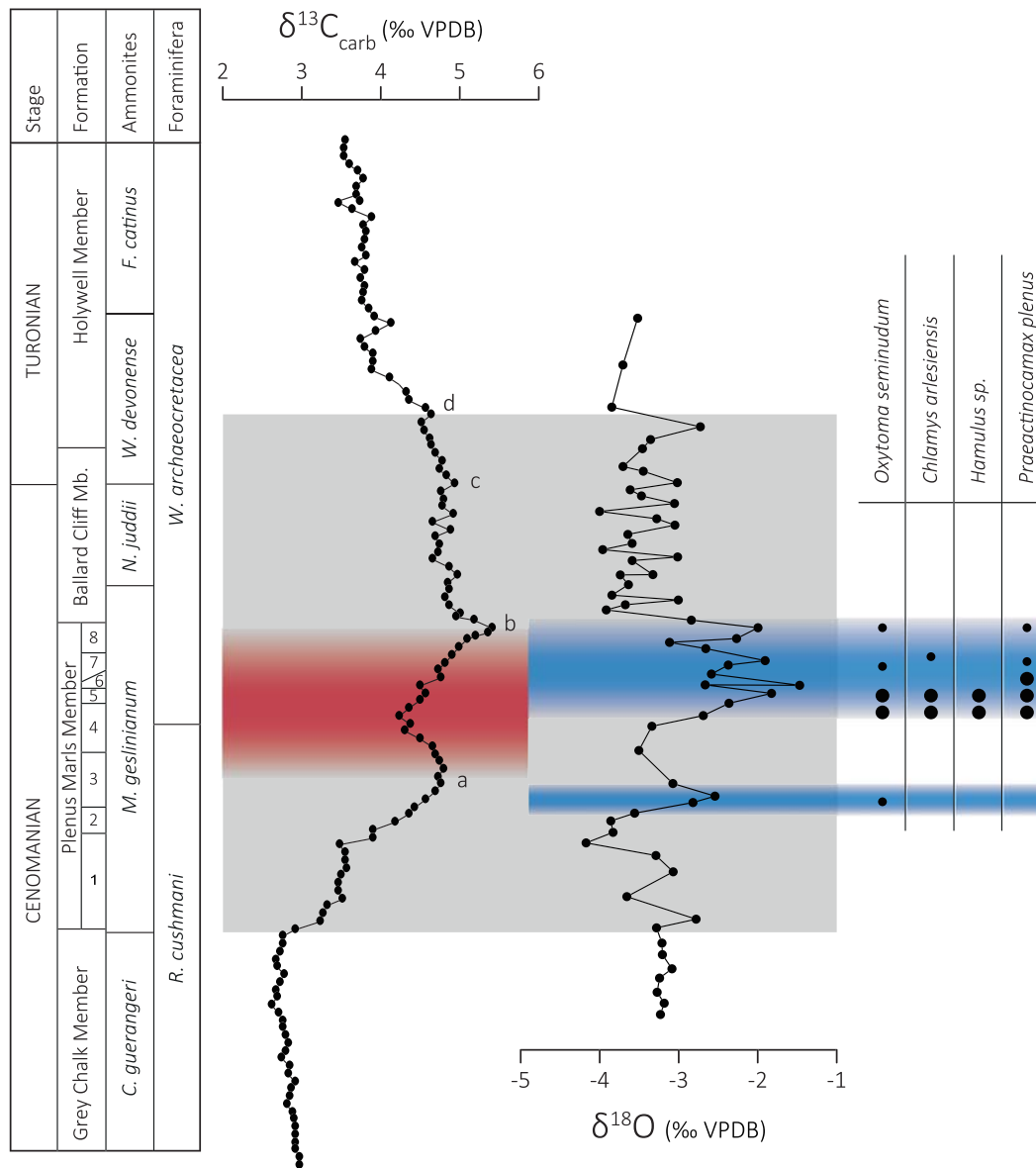


Figure 1. The composite “type-section” recording OAE 2 and the Plenus Cold Event from the English Chalk, using $\delta^{13}\text{C}_{\text{carb}}$ from Eastbourne (Tsikos et al., 2004), and bulk $\delta^{18}\text{O}$ and boreal fauna from Dover (Gale & Christensen, 1996; Lamolda et al., 1994), correlated using the beds of the Plenus Marl member (for details see Jarvis et al., 2006). Points “a–d” show globally consistent positions on the $\delta^{13}\text{C}$ curve (Jarvis et al., 2006). The gray box shows the interval of OAE 2 (Jenkyns et al., 2017) extending from the uppermost Cenomanian to the lowermost Turonian. The red band indicates the Plenus carbon-isotope excursion, as defined in this study. The blue bands indicate cooling, with the upper band defined in this study as the PCE in a strict sense (Gale & Christensen, 1996).

recognized, and to contextualize these data by synthesizing all available records to investigate the global responses of carbon-cycling, temperature, and seawater chemistry around the time of the PCE.

2. Materials and Methods

2.1. Plenus Marls, Dover

This study was conducted on the ~3 m-thick Plenus Marls section near Shakespeare Cliff (Dover, UK; Figure 1), a well-known section for the study of OAE 2 (Schlanger et al., 1987). This site was located at a paleo-latitude of ~42°N during the OAE (van Hinsbergen et al., 2015), within the main part of the Anglo-Paris Basin. Across the basin, the Plenus Marls generally consist of a discrete unit of clay-rich chalks sandwiched between clay-poor chalks; the section at Dover comprises rhythmically bedded chalks and marls, rich in

planktic foraminifera, nannofossils, macrofauna, and clays (Jeans et al., 1991; Jefferies, 1962, 1963). Jefferies (1962, 1963) introduced a numbering system for these beds (numbered 1–8), which has been generally adopted and followed in this study. The Shakespeare Cliff exposure at Dover is one of the best onshore sections for geochemical studies, as there has been relatively little diagenetic alteration of the chalk (Scholle, 1974). Previous studies argued that, although foraminiferal $\delta^{18}\text{O}$ had been lowered by burial diagenesis, the relative trends were still reliable for paleoclimatic interpretation (Corfield et al., 1990; Jeans et al., 1991; Jenkyns et al., 1994; Lamolda et al., 1994).

The Plenus Marls were deposited in an epicontinental pelagic shelf sea during a major transgressive phase (Hancock, 1993). During the mid-Cretaceous, this location was connected with the Boreal Sea to the north, the Tethys to the south, and the North Atlantic to the west (Hancock, 1975; Hancock & Kauffman, 1979).

2.2. Sampling and Sample Preparation

Samples were collected every 10 cm from above and below the erosional base of the Plenus Marls up to Bed 8, with two additional samples at a 30 cm spacing from the overlying chalk. Samples were oven-dried for 48 hr at 40 °C to remove residual water and the edges were scraped clean using a metal spatula to remove any loose rock debris or other detritus. Samples were then ground to a fine powder using an agate pestle and mortar, and homogenized.

2.3. Stable Carbon and Oxygen Isotopes

Bulk carbonate samples were oxidized to remove organic matter by means of H_2O_2 (15%, pH 8) being added to each sample and allowed to react for 30 min, then oven-dried at 40 °C. Measurements were performed on a Delta V Advantage isotope mass spectrometer fitted with a Gas Bench II in the Department of Earth Sciences (University of Oxford); the carbonates were converted to CO_2 with 100% H_3PO_4 . Three internal standards were used that have previously been calibrated to international reference materials: CarreraCam, Wiley, and NOCZ ($n = 2, 2, 5$, respectively). Respective $\pm 1\sigma$ values are 0.04, 0.02, and 0.03% for $\delta^{13}\text{C}$, and 0.02, 0.07, and 0.02% for $\delta^{18}\text{O}$. In-house marble standard NOCZ has a long-term external repeatability of 0.07% for $\delta^{13}\text{C}$ and 0.09 for $\delta^{18}\text{O}$. The $\delta^{18}\text{O}$ and $\delta^{13}\text{C}$ values are expressed in per mil variations relative to VPDB.

2.4. Neodymium Isotopes

Nd was extracted from bulk chalk using the method of Zheng et al. (2013), followed by the standard two-stage ion-exchange column separation technique (Pin & Zalduegui, 1997). In short, 20 mL of 10% acetic acid was added to 5 g of powdered sample, and allowed to react for 2 hr. The samples were centrifuged, after which the supernatant was pipetted off, dried down, re-dissolved in 6 M HCl and dried down again, and finally re-dissolved in 1 M HCl before column chemistry. Rare earth elements were separated from major cations using 0.8 mL AG50W-X12 (200–400 μm) resin with 6 M HNO_3 as an eluent. On a second column, Nd was separated from other REEs using 125 μL of Ln spec (20–40 μm) resin with 0.25 M HCl as an eluent.

Nd isotopes ($\epsilon_{\text{Nd}(t)}$) were analyzed on an MC-ICP-MS (NuPlasma) in the Department of Earth Sciences (University of Oxford). Mass bias was corrected by using $^{146}\text{Nd}/^{144}\text{Nd} = 0.7219$ with an exponential law. Samples were measured by bracketing with the JNdi-1 Nd isotope standard, and the instrument drift was corrected by normalizing $^{143}\text{Nd}/^{144}\text{Nd}$ ratios of the bracketing JNdi-1 to a reference value of 0.512115 (Tanaka et al., 2000). Total procedural blanks yielded ≤ 355 pg Nd, which is negligible compared to the minimum sample yield of 27 ppb Nd (sample DPM 140). The JNdi-1 standard had an external long-term reproducibility of $\sim 0.4 \epsilon_{\text{Nd}}$ (2σ), without application of a drift correction.

2.5. Chromium and Rare Earth Element Concentrations

Approximately 0.01 g of the bulk carbonate sample was dissolved in 0.5 M acetic acid. The solutions so produced were subsequently dried down and re-dissolved in 2% HNO_3 to form a solution containing approximately 100 ppm Ca. Standard solution mixtures containing a suite of synthetic standards of 40 trace elements including chromium and the rare earth elements (REE) and doped with 100 ppm Ca were used to produce a calibration curve. Cr, Ce, Pr, and Nd concentrations were measured on an Agilent 7500 s ICP-QQQ-MS at the Open University in O_2 and He collision mode, respectively. Cerium concentrations were normalized to post-Archaeon Australian Shale (PAAS) concentrations (Taylor & McLennan, 1995). Cerium anomalies are expressed as $\text{Ce}/\text{Ce}^* = (\text{Ce}_{\text{sample}}/\text{Ce}_{\text{PAAS}})/[\text{Pr}_{\text{sample}}/\text{Pr}_{\text{PAAS}} * (\text{Pr}_{\text{sample}}/\text{Pr}_{\text{PAAS}})]/(\text{Nd}_{\text{sample}}/$

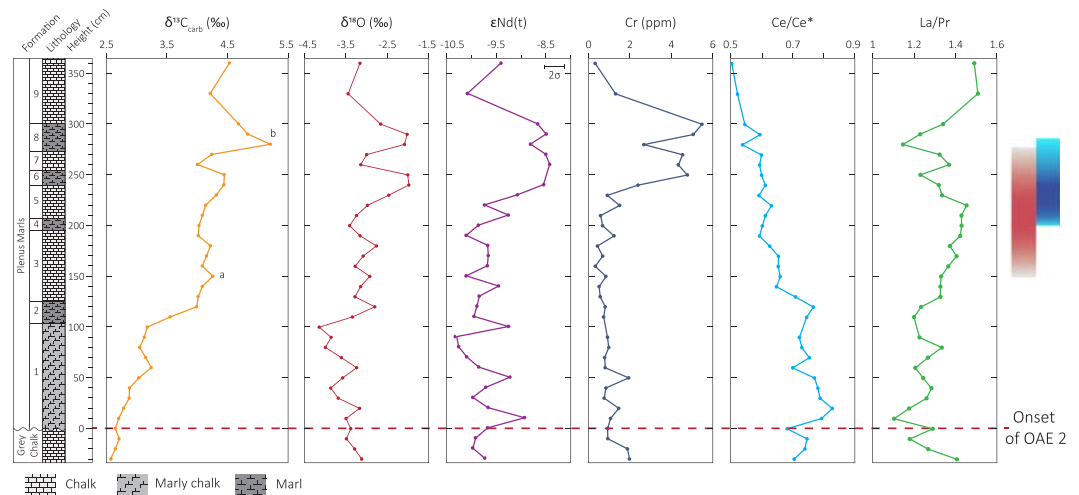


Figure 2. New geochemical data from the Plenus marls at Dover, UK. Points “a” and “b” are identified on the $\delta^{13}\text{C}$ curve. With the exception of ϵ_{Nd} , error bands are smaller than the data points. The red dotted line indicates the onset of OAE 2, the red band indicates the Plenus carbon-isotope excursion, and the blue band indicates the PCE in a strict sense.

Nd_{PAAS}] (Tostevin et al., 2016). Measurements are reproducible within 2% for Cr and 9% for Ce/Ce* based on replicate analyses of JDO-1 (a carbonate standard reference material).

3. Results

3.1. Stable Carbon and Oxygen Isotopes

The $\delta^{13}\text{C}_{\text{carb}}$ ranges from 2.57 to 5.21‰ (Figure 2), with a minor negative excursion at the level of the lower-middle part of Bed 7 in the Plenus Marls. The record shows positive shifts at Beds 3 (peak “a”) and 8 (peak “b”), although the trough between Beds 4 and 8 is not well expressed. The excursion documented here corresponds to excursions seen in other $\delta^{13}\text{C}_{\text{carb}}$ records from Dover and Eastbourne (Gale et al., 2005; Gale & Christensen, 1996; Jarvis et al., 1988; Jeans et al., 1991; Lamolda et al., 1994; Paul et al., 1999; Pearce et al., 2009; Tsikos et al., 2004; Voigt et al., 2006; Zheng et al., 2016).

The new Dover record shows $\delta^{18}\text{O}$ varying between -4.14 and -1.98 ‰ with a positive shift at Bed 2 and a more significant positive excursion across Beds 6–8 characterized by a double peak indicating two phases of relatively greater $\delta^{18}\text{O}$ values, which coincide with the main marls (Figure 2).

3.2. Neodymium Isotopes

Thirty-five samples had sufficient neodymium concentrations to allow measurement of Nd isotopes, which ranged from -10.3 to -8.4 ϵ units (Figure 2). This record shows a well-resolved 1.5 ϵ unit positive excursion, synchronous with the main cooling event, suggesting a change in water mass chemistry in the Chalk Sea across southern England in the latest Cenomanian. The timing and magnitude of the positive excursion correlates well with the ϵ_{Nd} record from Eastbourne; however, the new data do not show the earlier negative excursion recorded in Beds 2–4 at Eastbourne (Zheng et al., 2013), possibly owing to the presence of hiatuses and condensed horizons in the Dover section (cf. Gale et al., 1993; Jarvis et al., 2006). In a previous study of the Plenus Marls at Eastbourne, fish debris and bulk carbonates from the same stratigraphic levels were found to record nearly identical $\epsilon_{\text{Nd}(t)}$ values (Zheng et al., 2013, 2016). As such, the $\epsilon_{\text{Nd}(t)}$ record here is interpreted dominantly to reflect bottom-water values.

3.3. Chromium and Cerium Concentrations

Chromium and REE concentrations were determined in 35 samples, with chromium concentrations ranging from 0.32 to 5.48 ppm, with the highest values found in Beds 6–8 of the Plenus Marls (Figure 2). Chromium concentrations peak during the uppermost Plenus interval, reflecting the pattern observed in $\delta^{18}\text{O}$. However, the response of Cr lags slightly behind the peaks in $\delta^{18}\text{O}$. Previous studies on the Plenus Marls

at Eastbourne, Sussex have also identified pulses of Cr enrichment during the Plenus interval (Orth et al., 1993; Pearce et al., 2009; Jenkyns et al., 2017).

REE patterns yielded Ce/Ce* data with Ce anomalies between 0.5 and 0.85. The Ce/Ce* anomalies generally decrease upsection, mirroring the generally increasing pattern of $\delta^{13}\text{C}$. While Cerium anomalies are lower during the Plenus interval than prior to the event, there are no observable excursions superimposed onto the decreasing trend (cf. Lu et al., 2010).

4. Discussion of Plenus Cold Event Records

Because the Plenus event was first identified in the Chalk of southern England, these exposures will be considered as comprising a composite type-section (Figure 1), using the $\delta^{13}\text{C}_{\text{carb}}$ record of Tsikos et al. (2004) from Eastbourne and the $\delta^{18}\text{O}$ record of Lamolda et al. (1994) from Dover, which also yielded the boreal fauna identified by Gale and Christensen (1996). All other records will be correlated to and compared with this composite record. The negative $\delta^{13}\text{C}$ excursion between peaks “a” and “b” is henceforth referred to as the Plenus carbon-isotope excursion (P-CIE), and the interval of cooling during the “second buildup” will be called the Plenus Cold Event, in a strict sense (after Gale & Christensen, 1996). Using this definition, and based on the age model of Kuhnt et al. (2017), the P-CIE lasted ~65 kyr, while the main phase of the cooling (as seen at Eastbourne) lasted ~40 kyr.

4.1. Evidence for Change in the Carbon Cycle

Across the globe, negative carbon-isotope excursions recording the P-CIE are registered in bulk carbonate, bulk marine and terrestrial organic matter, and compound-specific materials (Figure 3). Notably, the Plenus CIE shows remarkable consistency in its timing and expression across the world in terms of its relationship to, and position in, the overarching positive excursion characteristic of the Cenomanian–Turonian interval. However, care must be taken when interpreting these records in terms of global changes in carbon cycling as local processes may overprint any global signal. For example, short-term local variations in $\delta^{13}\text{C}$ may reflect a direct response to transgression–regression cycles, which affect the area of shelf and marginal seas as major sinks for organic matter, or changes in oceanic ^{12}C storage in response to changing ocean circulation (Jenkyns et al., 1994; Voigt, 2000). Changes in local upwelling may also affect the $\delta^{13}\text{C}$ record, with waters coming from oxygen-minimum zones having lower seawater $\delta^{13}\text{C}$ than near-surface dissolved inorganic carbon (Berger & Vincent, 1986). As such, local oceanographic feedback may have produced carbon-isotope excursions partially decoupled from the isotopic composition of the global ocean–atmosphere carbon reservoir.

The carbon-isotope signature of bulk organic matter is especially susceptible to modification by shifts in its composition due to changes in source, preservation, and diagenetic alteration (e.g., Voigt et al., 2006). In many studies, diagenesis has been noted as potentially producing false excursions that make it difficult to determine whether the $\delta^{13}\text{C}_{\text{org}}$ records reflect paleoenvironmental change or simply local overprinting (Jarvis et al., 2006; Voigt, 2000; Voigt et al., 2006). Changing the ratio of terrestrial to marine organic matter, by either increased input or preferential preservation, will shift the $\delta^{13}\text{C}$ of the bulk material, potentially giving a false excursion unrelated to global or local carbon cycling. In several instances, bulk-organic and compound-specific $\delta^{13}\text{C}$ records from a single section show differences between these archives in the structure of the excursion through the OAE 2 interval (e.g., ODP Site 1276, Cape Verde Basin; Sinninghe Damsté et al., 2010; Figure 4), possibly owing to differences in local carbon-cycle processes, as well as changes in the relative abundance of different organic components (Gale et al., 2019; Kolonic et al., 2005; Sinninghe Damsté et al., 2010; Tsikos et al., 2004). Furthermore, differences in the pattern of the $\delta^{13}\text{C}_{\text{carb}}$ and $\delta^{13}\text{C}_{\text{org}}$ curves can also be seen within a single section, such as at Tarfaya (Kuhnt et al., 2017; Tsikos et al., 2004), which may indicate variable fractionation between organic and inorganic carbon, local changes in carbon cycling, and/or possibly diagenetic overprints on the carbonate and/or organic fractions (Jarvis et al., 2006). However, allowing for minor differences due to the aforementioned factors, $\delta^{13}\text{C}$ curves show a generally globally consistent evolution across the OAE and Plenus interval at most localities.

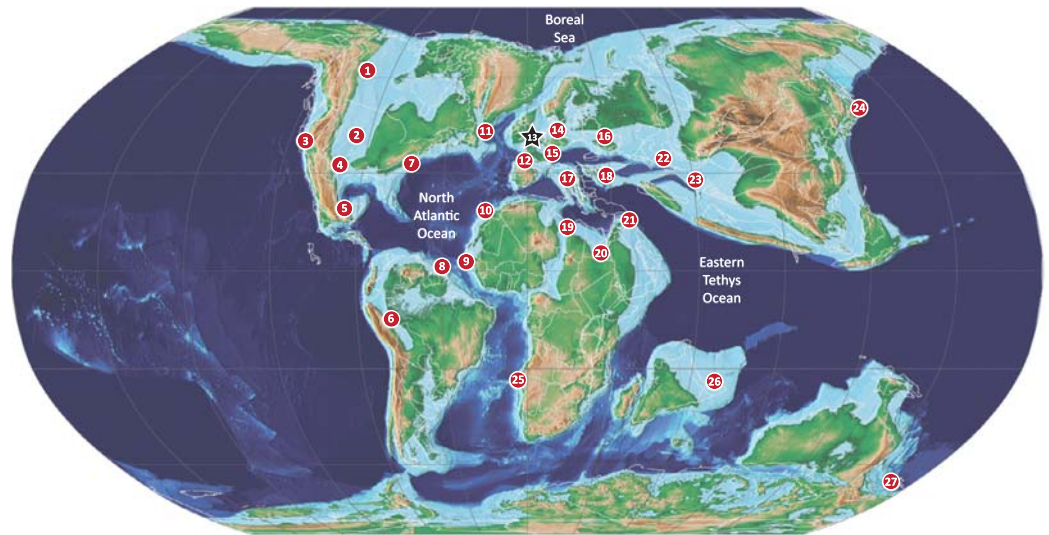


Figure 3. Global distribution of known records demonstrating the Plenian CIE (a negative $\delta^{13}\text{C}$ excursion between points “a” and “b” in Figure 1) or an excursion in CO_2 across the Plenian interval, as indicated by $\Delta^{13}\text{C}$, compound-specific $\delta^{13}\text{C}$, or leaf stomata. **1** Pratt’s landing (van Helmond et al., 2016); Vermillion River, Well 10–35–45–2WA (Prokoph et al., 2013). **2** Cuba, KS (Bowman & Bralower, 2005); Pueblo (Barclay et al., 2010; Bowman & Bralower, 2005; Caron et al., 2006; Keller et al., 2008; Pratt, 1985; Sageman et al., 2006); USGS Portland-1 core (Eldrett et al., 2017); Aristocrat Angus core (Joo & Sageman, 2014); Hot Springs, CO (Desmares et al., 2007); SH#1 core (Jones et al., 2019); generalized Western Interior Seaway (Orth et al., 1993). **3** Great Valley sequence, CA (Du Vivier et al., 2015). **4** Innes-1 core, Iona-1 core, Well X core (Eldrett et al., 2017). **5** Axaxacoalco, Barranca el Tigre, Barranco el Canon (Elrick et al., 2009). **6** Laurichochoa, Piedra Parada, Uchuchacua (Navarro-Ramirez et al., 2016, 2017). **7** Bass River, NJ (Bowman & Bralower, 2005; van Helmond et al., 2013). **8** ODP Site 1258 (Erbacher et al., 2005); ODP Site 1260 (Eldrett et al., 2017; Erbacher et al., 2005; Forster et al., 2007; Van Bentum et al., 2012); ODP Site 1261 (Eldrett et al., 2017; Erbacher et al., 2005). **9** DSDP Site 367 (Dickson et al., 2016; Forster et al., 2007; Kuypers et al., 1999; Sinninghe Damsté et al., 2008). **10** Tarfaya (Keller et al., 2008; Kolonic et al., 2005; Kuhnt et al., 2017; Kuypers et al., 2002; Tsikos et al., 2004); Mpl, S57, S75 (Kolonic et al., 2005); S13 (Kolonic et al., 2005; Kuypers et al., 1999). **11** ODP Site 1276 (Sinninghe Damsté et al., 2008; van Helmond et al., 2014). **12** Arobes, Ganuza, Menoyo (Kaiho et al., 2014); Manilvala (Mort et al., 2007); Puentedey (Barroso-Barcenilla et al., 2011). **13** Dover (this study; Jeans et al., 1991; Lamolda et al., 1994); Eastbourne (Gale et al., 2005; Jenkyns et al., 1994; Paul et al., 1999; Pearce et al., 2009; Tsikos et al., 2004; Zheng et al., 2013); Culver cliff (Jarvis et al., 2001). **14** Gröbern (Voigt et al., 2006); Halle (Voigt et al., 2007); Wunstorf (Du Vivier et al., 2014; Voigt et al., 2008); Roter Sattel (Charbonnier et al., 2018). **15** Lambruisse (Takashima et al., 2009); Pont d’Issole (Grosheny et al., 2006; Jarvis et al., 2011); Les Lattes, Le Bourgeut (Grosheny et al., 2017); Cassis (Heimhofer et al., 2018); Clot Chevalier (Gale et al., 2019). **16** Pecinov, Czech Republic (Košfák et al., 2018). **17** Bottaccione (Kuroda et al., 2007); Furlo (Mort et al., 2007); Gubbio (Jenkyns et al., 1994; Tsikos et al., 2004); Raia del Pedale (Owens et al., 2013); Monte Coccovello, Monte Varchera (Parente et al., 2008). **18** Crimea (Fisher et al., 2005). **19** Jerissa (Zaghib-Turki & Soua, 2013); Oued Mellegue (Nederbragt & Fiorentino, 1999); Wadi Bahoul (Caron et al., 2006). **20** Wadi Feiran (El-Sabbagh et al., 2011). **21** Ghawr Al Mazar (Wendler et al., 2016); Wadi Karak (Farouk et al., 2017). **22** Aimaki, Khadzalmakhi, Levashi (Gavrilov et al., 2013). **23** Taherabad (Kalanat et al., 2018). **24** Tappu (Nemoto & Hasegawa, 2011); Yezo (Du Vivier et al., 2015). **25** ODP Site 530 (Forster et al., 2008). **26** Gongzha (Bomou et al., 2013); Tingri (Li et al., 2006). **27** Sawpit Gully, Mangaotane B (Gangl et al., 2019; Hasegawa et al., 2013); Mangaotane A (Hasegawa et al., 2013). Base map from Scotese, (2014).

4.1.1. Evidence for Change in CO_2

Reconstructions of atmospheric CO_2 across OAE 2 are few in number (Figure 5) and, in some cases, open to interpretation. A reconstruction of $p\text{CO}_2$ based upon values of the stomatal index of fossil leaves from the margins of the Western Interior Seaway indicates two increases in $p\text{CO}_2$ values during the early stages of OAE 2, coincident with negative $\delta^{13}\text{C}_{\text{org}}$ excursions (Barclay et al., 2010). These authors do not specify which event they think correlates with the PCE, but do interpret the increased stomatal index values as reflecting a global decrease in atmospheric $p\text{CO}_2$ in response to carbon burial. Using integrated biostratigraphy and chemostratigraphy, we interpret the P-CIE as the negative $\delta^{13}\text{C}$ excursion between 25- and 50-m height (Figure 5; cf. Laurin et al., 2019), consistent with the interpretation of Jarvis et al. (2011). While the stomatal data are very sparse across this interval, atmospheric CO_2 appears to rise from point “a” (Figure 5). Regardless of which negative excursion is interpreted to be the P-CIE, a fall in $\delta^{13}\text{C}$ correlates with a rise

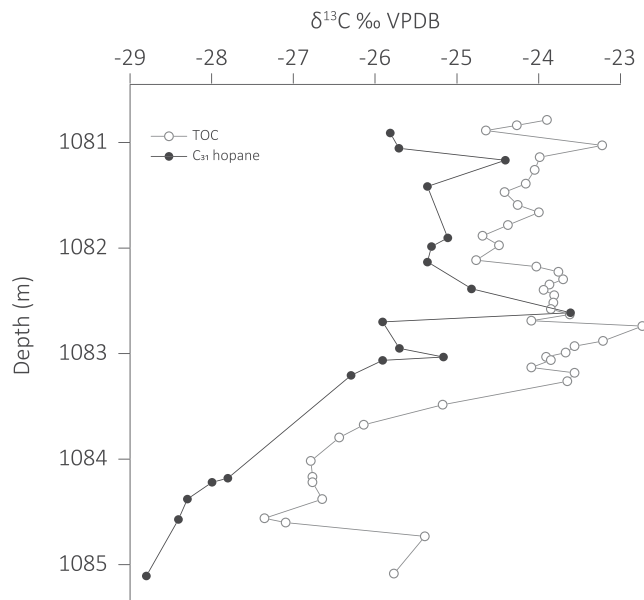


Figure 4. Comparison of $\delta^{13}\text{C}_{\text{org}}$ and $\delta^{13}\text{C}_{\text{hopane}}$ records from ODP Site 1276, Cape Verde Basin (adapted from Sinninghe Damsté et al., 2010) demonstrating a stratigraphic offset in the position of the negative excursion seen in $\delta^{13}\text{C}_{\text{org}}$ at $\sim 1,083.1$ m below sea floor and in $\delta^{13}\text{C}_{\text{hopane}}$ at $\sim 1,082.8$ m below sea floor.

in $p\text{CO}_2$. Leaf-wax $\delta^{13}\text{C}$ records from the Cenomanian–Turonian organic-rich sediments from the equatorial Atlantic (Kuypers et al., 1999; Sinninghe Damsté et al., 2010) and France (Heimhofer et al., 2018) suggest a rise in CO_2 from point “a” to the trough of the P-CIE and then a fall to point “b” (Figure 5). Given the similarity in CO_2 trends indicated by these two independent proxies for atmospheric CO_2 , we suggest that the rise in $p\text{CO}_2$ from point “a” and fall across point “b” likely reflect global changes in the atmosphere.

$\Delta^{13}\text{C}$ (the offset between $\delta^{13}\text{C}_{\text{carb}}$ and $\delta^{13}\text{C}_{\text{org}}$ in marine sediments) reflects the degree of carbon fractionation during photosynthesis, which is $p\text{CO}_2$ -dependent (Farquhar et al., 1989; Freeman & Hayes, 1992). $\Delta^{13}\text{C}$ records changes in dissolved seawater CO_2 concentration, which is assumed to be in equilibrium with atmospheric CO_2 , and thus can be used as a $p\text{CO}_2$ proxy. $\Delta^{13}\text{C}$ marine records from the UK, France, Germany, and Morocco show a similar trend to the terrestrial records from the Western Interior Seaway: namely, a rise then fall in CO_2 over the P-CIE interval (Gale et al., 2005; Jarvis et al., 2011; Voigt et al., 2006, 2007). Two $\Delta^{13}\text{C}$ records, from France (Gale et al., 2019) and Iran (Kalanat et al., 2018), show different trends: both indicate an increase in $p\text{CO}_2$ over the P-CIE, although both show poorly resolved Plenian CIEs owing to condensation, diagenesis, or poorly resolved stratigraphy.

Despite their general agreement with the terrestrial proxies for $p\text{CO}_2$, $\Delta^{13}\text{C}$ records must be treated with some caution when interpreted in the

context of atmospheric CO_2 changes. Changes in oceanography may have generated local variations in ocean CO_2 fluxes and concentrations. For example, the incursion of a cold, oxygenated water mass across a region would have led to the remineralization of buried organic matter, causing a localized increase in $[\text{CO}_2]$ in bottom waters and potentially, particularly in areas of upwelling, to CO_2 outgassing to the atmosphere. As the total organic carbon (TOC) content of strata varied regionally, the degree of remineralization would have varied between sites, producing different CO_2 concentrations in different locations. Furthermore, as CO_2 solubility is dependent on water temperature (e.g., Broecker & Peng, 1974), a cold water mass would contain higher concentrations of dissolved CO_2 compared with warmer waters, and this alone would have affected the local pH without involving any atmospheric processes. Euxinic conditions may also affect local CO_2 concentrations, as the degradation of organic matter allows phosphate to be released back to bottom waters, driving increased productivity and organic-matter deposition (Jarvis et al., 2011; Mort et al., 2007). These local processes could potentially mask any signal of atmospheric $p\text{CO}_2$ change and, if not recognized, could lead to erroneous interpretations of the drivers of the PCE.

4.2. Evidence for Changing Temperature

The Plenian Cold Event was first recognized based on the southerly migration of boreal fauna coincident with two positive $\delta^{18}\text{O}$ excursions in the Chalk of Dover, UK (Gale & Christensen, 1996; Jefferies, 1962). In the Dover Chalk records, cooling is observed in Beds 2 and 4–8 of the Plenian Marls (Figures 1 and 2), supported by numerous other records of faunal assemblages and $\delta^{18}\text{O}$ from southeast England, with some variation in the timing of the onset of cooling (this study; Gale et al., 2005; Jeans et al., 1991; Jefferies, 1962, 1963; Lamolda et al., 1994; Paul et al., 1999; Tsikos et al., 2004; Voigt et al., 2004, 2006). The main phase of cooling in southeast England, as exemplified by the carbon-isotope record, extends from the trough of the P-CIE to point “b”.

The early stages of OAE 2 have been studied extensively across the Northern Hemisphere, with multiple quantitative and qualitative records indicating brief cooling around the P-CIE interval (Figure 6). $\delta^{18}\text{O}$ (Kalanat et al., 2018; Kuhnt et al., 2017), TEX_{86} (Forster et al., 2007; Sinninghe Damsté et al., 2010), faunal assemblages (Eldrett et al., 2017; van Helmond et al., 2013, 2016), and foraminiferal coiling direction (Desmares et al., 2016) show clear evidence for cooling across the Tethyan margins, North Atlantic, and Western Interior Seaway. In France and Germany, incursions of boreal fauna and dinocysts also indicate cooling, as supported by $\delta^{18}\text{O}$ and TEX_{86} records (Figure 7; Takashima et al., 2009; Voigt et al., 2006,

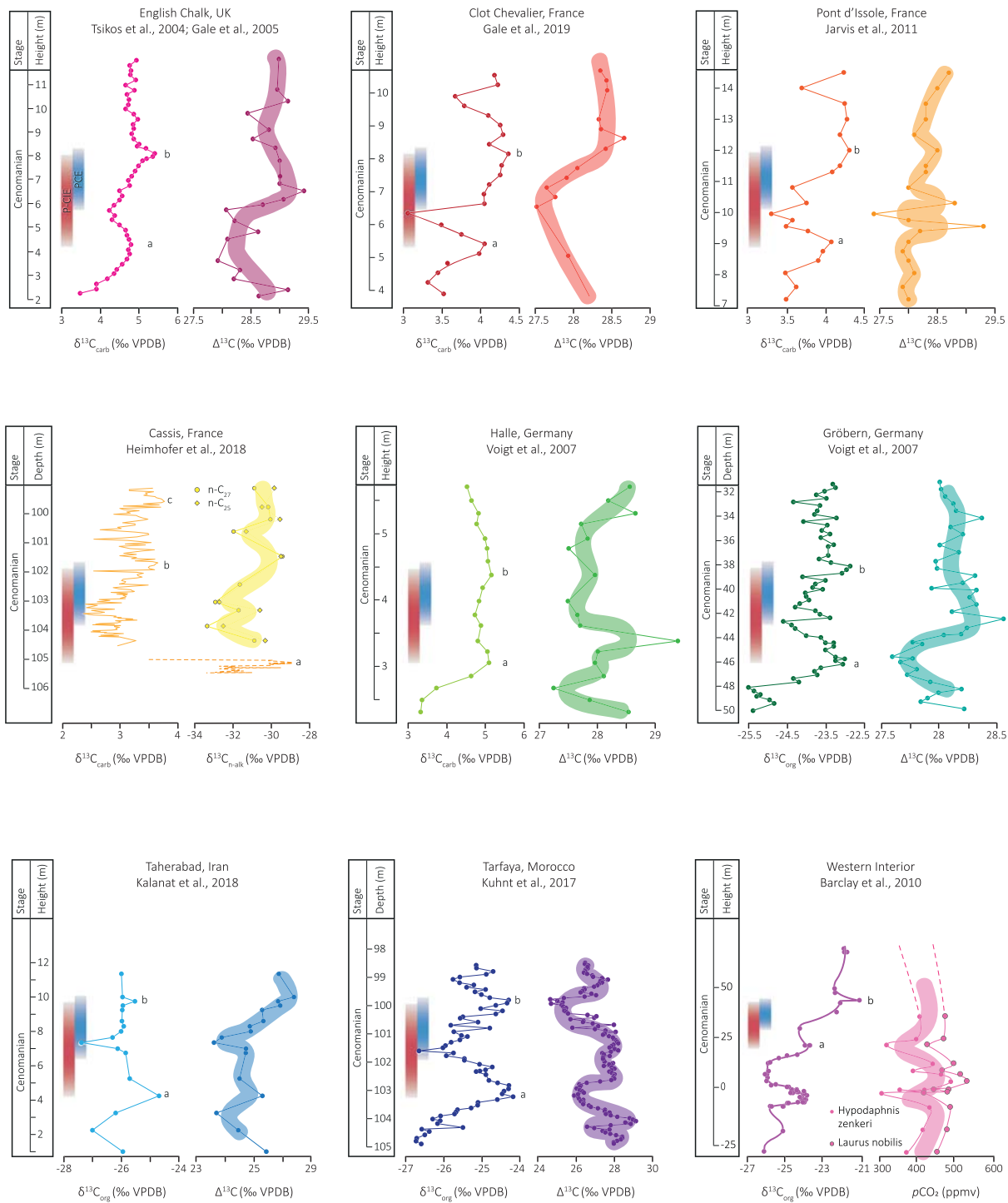


Figure 5. Records of CO₂ change across the Plenius interval. The red bands indicate the P-CIE, and the blue bands indicate the PCE in a strict sense; points “a” to “c” of the OAE are labeled. Colored bands illustrate visual approximations of trends.

2007, 2008; van Helmond et al., 2015). However, some bulk δ¹⁸O records from hemipelagic clay-rich carbonates (e.g., Pont d’Issole, Vocontian Basin, France) show no clear excursion across the PCE interval (Jarvis et al., 2011; Voigt et al., 2006), even though nearby sections, a few tens of kilometers away, show distinct positive excursions of 1–1.5‰ locally alongside qualitative measures of cooling, such as changes in the direction of foraminiferal coiling (Gale et al., 2019; Grosheny et al., 2017).

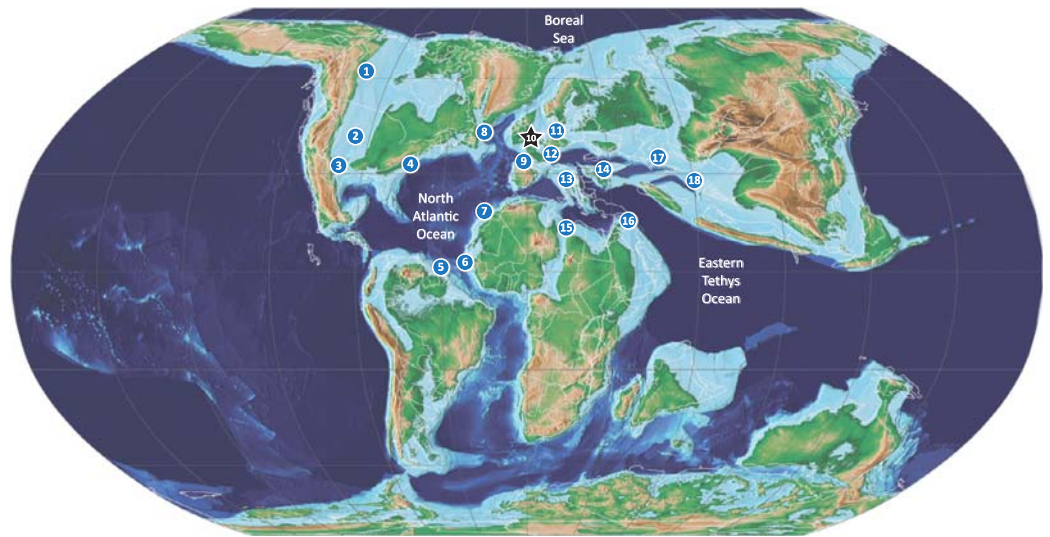


Figure 6. Global distribution of known records demonstrating a change in temperature across the PCE interval, based on records of TEX_{86} , $\delta^{18}\text{O}$, faunal assemblages, and foraminiferal coiling. **1** Pratt's Landing (van Helmond et al., 2016). **2** Hot Springs, SD (Desmares et al., 2016); Pueblo (Caron et al., 2006; Desmares et al., 2016); USGS Portland-1 Core (Eldrett et al., 2017). **3** Iona-1 core, Innes-1 core, Well X core (Eldrett et al., 2017). **4** Bass River, NJ (van Helmond et al., 2013). **5** ODP site 1260 (Eldrett et al., 2017; Forster et al., 2007). **6** DSDP Site 367 (Forster et al., 2007). **7** Tarfaya (Kuhnt et al., 2017; Tsikos et al., 2004). **8** ODP Site 1276 (Sinninghe Damsté et al., 2008). **9** Arabes, Ganuza, Menoyo (Kaiho et al., 2014); Puentevedy (Barroso-Barcenilla et al., 2011). **10** Dover (this study; Jefferies, 1962; Jeans et al., 1991; Lamolda et al., 1994); Eastbourne (Jenkyns et al., 1994; Paul et al., 1999; Pearce et al., 2009; Tsikos et al., 2004; Voigt et al., 2004, 2006; Zheng et al., 2013). **11** Gröbern (Voigt et al., 2006); Halle (Voigt et al., 2007); Wunstorf (van Helmond et al., 2015). **12** Cassis (Heimhofer et al., 2018); Clot Chevalier (Gale et al., 2019); Lambrousse (Takashima et al., 2009); Les Lattes (Gale & Christensen, 1996); Pont d'Issole (Jarvis et al., 2011). **13** Gubbio (Jenkyns et al., 1994). **14** Crimea (Fisher et al., 2005). **15** Oued Mellegue (Nederbragt & Fiorentino, 1999); Wadi Bahoul (Caron et al., 2006). **16** Wadi Karak (Farouk et al., 2017). **17** Amaki, Khadzalmakhi, Levashi (Gavrilov et al., 2013). **18** Taherabad (Kalanat et al., 2018). Base map from Scotese, (2014).

Although cooling appears to be geographically widespread, the precise timing of the falls in local paleotemperature is not consistent globally, or even within a single basin. For example, in Germany, Pueblo and DSDP Site 367, cooling starts well before the P-CIE and reaches its lowest temperature around point “a,” based on TEX_{86} , $\delta^{18}\text{O}$, foraminiferal coiling, and faunal assemblages (Figure 7; Voigt et al., 2007; Forster et al., 2007; van Helmond et al., 2015; Desmares et al., 2016). By contrast, in the Chalk records from southern England, and TEX_{86} records from DSDP Site 367 (equatorial Atlantic) and ODP Site 1276 (North Atlantic), the cooling apparently started later and peaked around point “b” (Forster et al., 2007; Gale & Christensen, 1996; Lamolda et al., 1994; Sinninghe Damsté et al., 2010). Other sites, such as Tarfaya and ODP Site 1260, suggest a more complex pattern of cooling, with multiple excursions in the TEX_{86} and $\delta^{18}\text{O}$ records (Forster et al., 2007; Kuhnt et al., 2017). However, Tarfaya is recognized as a paleo-upwelling area, which would have complicated the SST response (e.g., Einsele & Wiedmann, 1982; Kolonic et al., 2005). Although local diagenesis may have affected some of the SST records, in particular those deriving from oxygen isotopes, the existence of consistent differences in the relative timing between carbon-isotope events and local paleotemperature minima (based on both geochemical and paleontological proxies) suggests that the cooling of water masses was diachronous.

4.3. Evidence for Changing Water Mass Character

Geochemical, lithological, and faunal records across OAE 2 demonstrate significant and variable changes in water mass character associated with the event, variously attributed to changes in redox, circulation, and/or volcanic activity (Figure 8; e.g., Eicher & Worstell, 1970; Orth et al., 1993; MacLeod et al., 2008; Martin et al., 2012; Thomas & Tilghman, 2014). However, few records are of sufficiently high resolution to both identify the Plenian interval and any oceanographic changes associated therewith and determine the precise cause of these changes.

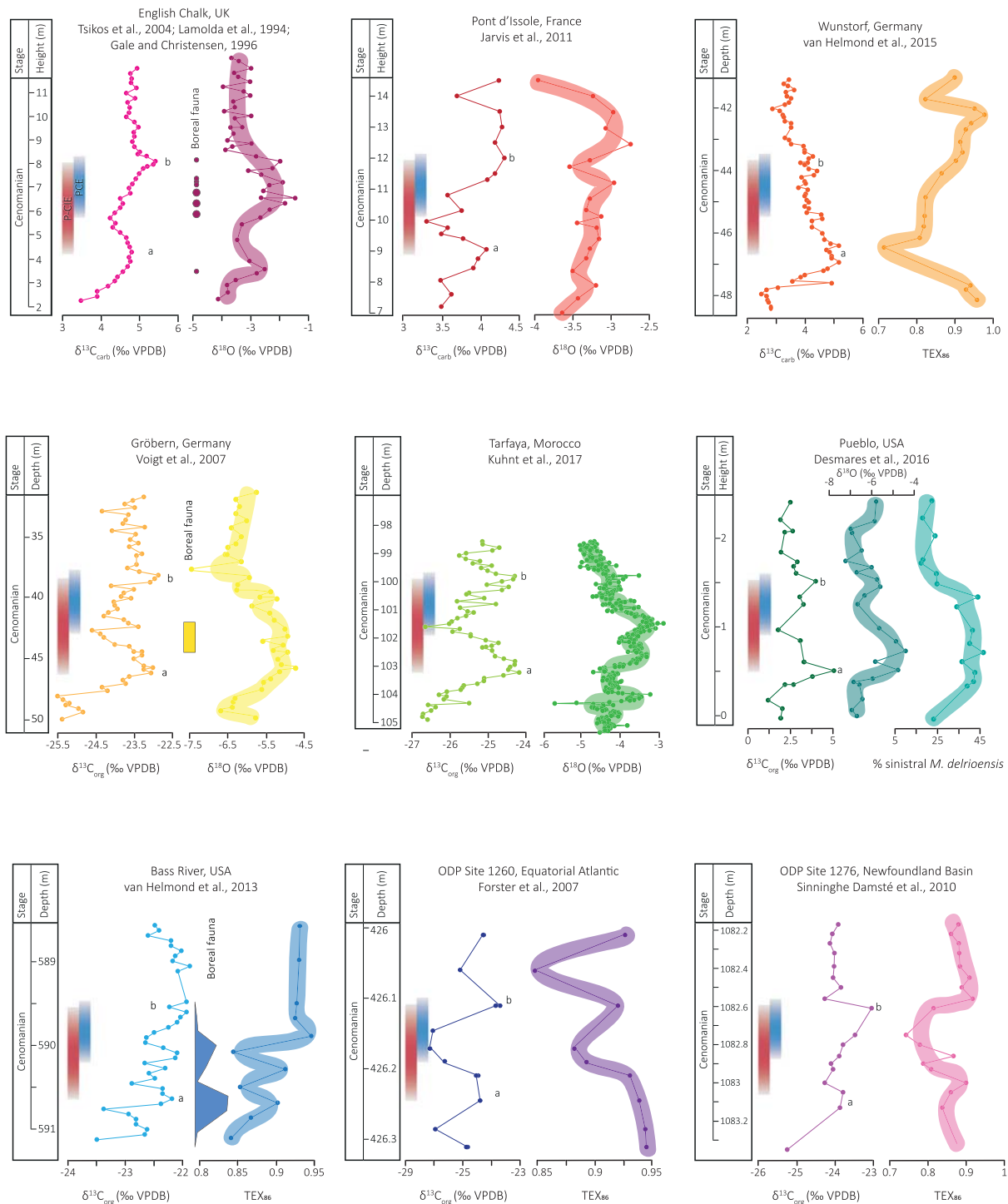


Figure 7. Records of SSTs during the Plenus interval. The red bands indicate the P-CIE, and the blue bands indicate the PCE in a strict sense; points “a” to “c” of the OAE are labeled. Dover stratigraphy from Lamolda et al. (1994); Wunstorf stratigraphy from Voigt et al. (2008). Colored bands illustrate visual approximations of trends.

Chromium is a redox-sensitive metal that may also be derived from basalt–seawater interactions, and as such is a useful tool for tracking changes in seawater chemistry (e.g., Bonnand et al., 2013; Holmden et al., 2016; Rimmelzwaal et al., 2019). At Dover in SW England, carbonate-fraction Cr concentrations show an approximately fivefold increase over the uppermost marls (this study; Figure 2). Similar spikes

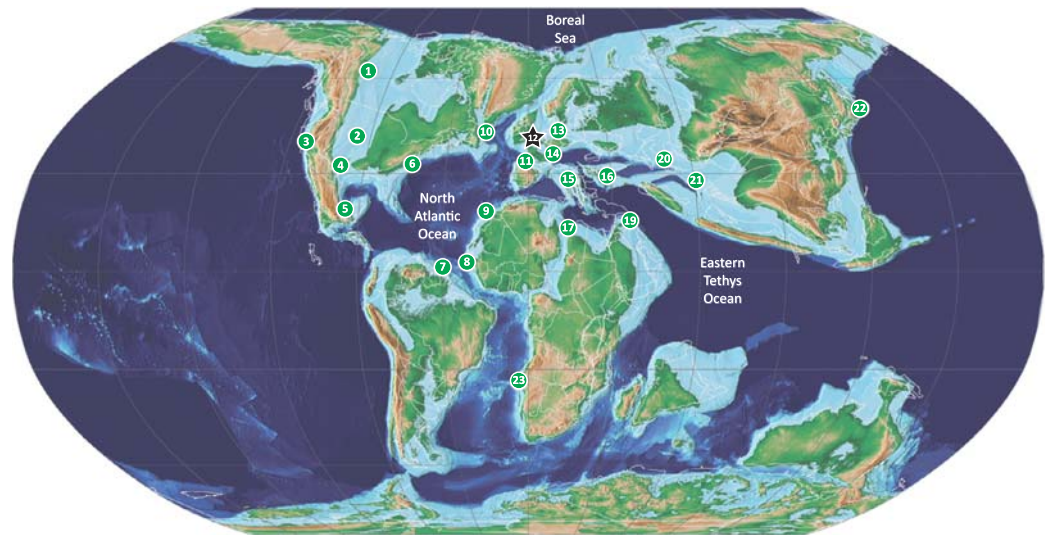


Figure 8. Global distribution of known records demonstrating a change in water mass character across the Plenius interval, as indicated by elemental, isotopic, lithological, or faunal changes in the sedimentary record. **1** Vermillion River (Prokoph et al., 2013). **2** Angus Aristocrat core (Zhou et al., 2015); Cuba, KS (Bowman & Bralower, 2005; Eldrett et al., 2014); Hot Springs, SD (Desmares et al., 2016); USGS Portland-1 core (Du Vivier et al., 2014; Eldrett et al., 2017; Holmden et al., 2016); generalized Western Interior Seaway (Orth et al., 1993); Pueblo (Bowman & Bralower, 2005; Caron et al., 2006; Keller et al., 2008; Elderbak et al., 2014). **3** Great Valley sequence, CA (Du Vivier et al., 2015). **4** Innes-1 core, Iona-1 core, Well X core (Eldrett et al., 2017). **5** Barranco el Canon (Elrick et al., 2009; Sweere et al., 2018). **6** Bass River, NJ (Bowman & Bralower, 2005). **7** ODP Site 1258 (Erbacher et al., 2005; Friedrich et al., 2006; Ostrander et al., 2017; Zhou et al., 2015); ODP Site 1260 (Du Vivier et al., 2014; Eldrett et al., 2017; Erbacher et al., 2005; Forster et al., 2007; Friedrich et al., 2006; Turgeon & Creaser, 2008); ODP Site 1261 (Erbacher et al., 2005; Friedrich et al., 2006). **8** DSDP Site 367 (Kuypers et al., 1999; Forster et al., 2007, 2008; Sinninghe Damsté et al., 2008; Du Vivier et al., 2014; Dickson et al., 2016). **9** Tarfaya (Dickson et al., 2016; Keller et al., 2008; Kuhnt et al., 2017; Kuypers et al., 2002; Tsikos et al., 2004); Mpl, S13, S57, S75 (Kolonik et al., 2005). **10** ODP Site 1276 (Sinninghe Damsté et al., 2008; van Helmond et al., 2014). **11** Puentedey (Barroso-Barcenilla et al., 2011); Arobes (Kaiho et al., 2014); Ganuza (Kaiho et al., 2014; Peryt & Lamolda, 1996); Manivala (Mort et al., 2007); Menoyo (Kaiho et al., 2014; Peryt & Lamolda, 1996). **12** Dover (this study; Jeans et al., 1991); Eastbourne (Clarkson et al., 2018; Lu et al., 2010; Orth et al., 1993; Owens et al., 2013; Paul et al., 1999; Pearce et al., 2009; Sweere et al., 2018; Zheng et al., 2013; Zhou et al., 2015). **13** Wunstorff (van Helmond et al., 2015); Halle (Voigt et al., 2007); Roter Sattel (Charbonnier et al., 2018); Wunstorff (Du Vivier et al., 2014; van Helmond et al., 2015). **14** Clot Chevalier (Gale et al., 2019); Lambrousse (Takashima et al., 2009); Le Bourgeut (Grosheny et al., 2017); Pont d'Issole (Danzelle et al., 2018; Grosheny et al., 2006; Jarvis et al., 2011); Vocontian Basin (Du Vivier et al., 2014). **15** Bottaccione (Kuroda et al., 2007); Furlo (Mort et al., 2007); Gubbio (Tsikos et al., 2004); Raia del Pedale (Clarkson et al., 2018; Owens et al., 2013; Sweere et al., 2018; Zhou et al., 2015). **16** Crimea (Fisher et al., 2005). **17** Oued Mellegue (Nederbragt & Fiorentino, 1999); Wadi Bahoul (Caron et al., 2006). **18** Wadi Feiran (El-Sabbagh et al., 2011). **19** Wadi Karak (Farouk et al., 2017). **20** Aimaki, Khadzhalmakhi, Levashi (Gavrilov et al., 2013). **21** Gharesu (Kalanat et al., 2016); Taherabad (Kalanat et al., 2016, 2017). **22** Tappu (Nemoto & Hasegawa, 2011); Yezo group (Du Vivier et al., 2015). **23** DSDP Site 530 (Du Vivier et al., 2014; Forster et al., 2008). **24** Gongzha (Bomou et al., 2013). Base map from Scotese, (2014).

in geochemical species (such as Cr, Mo, U, Mn) have been recorded at sites in the Chalk Sea and/or along the Tethyan margins (e.g., Orth et al., 1993; Jarvis et al., 2001; Kolonic et al., 2005; Pearce et al., 2009; Jenkyns et al., 2017; Charbonnier et al., 2018; Clarkson et al., 2018; Danzelle et al., 2018; Sweere et al., 2018; Gale et al., 2019), North Atlantic (Dickson et al., 2016; Eldrett et al., 2017; van Helmond et al., 2014), and the Western Interior Seaway (Eldrett et al., 2017; Holmden et al., 2016; Orth et al., 1993). These excursions have been attributed to a period of increased bottom-water oxygenation during which the remineralization of organic matter either released trace metals into the water column and/or removed anoxic/euxinic sinks for hydrothermally enriched bottom waters (Jenkyns et al., 2017). However, some sites show excursions in certain geochemical species but not others (e.g., Danzelle et al., 2018; Eldrett et al., 2017; Owens et al., 2013; Sweere et al., 2018). These differences may be due to the different reduction potentials of various elements and the local redox conditions pertaining at any one site. Local redox conditions during the Plenius interval may have prevented certain elements from being enriched in discrete reduced phases, such as in sulfides, or substituting in pyrite or

adsorbed onto organic matter but not allowed them to be incorporated in carbonates in more oxidized form even if present in relative abundance in seawater. Regardless of the cause, these variable expressions of redox change across the Plenus interval make it difficult to deconvolve global from local drivers of paleoenvironmental change.

Neodymium-isotope ratios, expressed as ϵ_{Nd} , are a powerful tool for reconstructing changes in past ocean circulation (Frank, 2002; Goldstein & Hemming, 2003). Roughly coeval with the Cr excursion in the Chalk of SW England, large ($\sim 1.5 \epsilon$ unit) excursions in neodymium isotopes across the PCE interval suggest changing circulation and/or possible input of magmatically derived radiogenic Nd (this study; Zheng et al., 2013, 2016). A link has been drawn between LIPs and oceanic anoxic events, particularly with respect to the Caribbean and High Arctic Large Igneous Provinces as possible triggers for OAE 2 (e.g., Snow et al., 2005; Tegner et al., 2011; Zheng et al., 2013). Osmium-isotope records from across the world have identified periods of volcanism or some form of basalt–seawater interaction around the Cenomanian–Turonian boundary, indicating likely LIP activity immediately prior to the onset of OAE 2 (Du Vivier et al., 2014, 2015; Scaife et al., 2017; Schröder-Adams et al., 2019; Turgeon & Creaser, 2008). Basalt–seawater interactions would not have just affected seawater Nd and Os but also other trace metals and isotopes, which further complicates the interpretation of their sedimentary records.

Ce anomalies reflect the oxidation state of seawater through the oxidation of Ce (III) to insoluble and particle-reactive Ce (IV) (De Baar et al., 1988; Zhou et al., 2015; Rimmelzwaal et al., 2019). In the Dover record, Ce* steadily decreases upsection, mirroring the generally increasing pattern of $\delta^{13}C$. These data can be compared with trace-element data from the Eastbourne section (Jenkyns et al., 2017; Lu et al., 2010). Cerium anomalies at Dover are generally lower during the PCE than prior to the event, but there is a significant increase in Ce/Ce* from 0.7 to 0.83 at the beginning of the OAE event in the Dover section. This rise is consistent with Mn/Ca data for the Eastbourne section, suggestive of an initial move to a less oxic seafloor, whereas the overall decrease in Ce/Ce*, particularly during the PCE, is consistent with I/Ca ratios indicating a move to more oxic surface waters at this time (Lu et al., 2010). Seawater and carbonates in modern marine environments commonly have both Ce and La anomalies and this is best demonstrated by calculating Ce/Ce* and Pr/Pr* values, which also covary with each other (Webb & Kamber, 2000). Our new carbonate record indicates that the late Cenomanian seawater also has both Ce and La anomalies. While Ce/Ce* and Pr/Pr* (supp. info.) values vary smoothly through the section, they are principally indicative of variable redox conditions, whereas La/Pr ratios still retain information about source input and are much more variable. In this case, the La/Pr ratio is a useful guide to the amount of basaltic input to the seawater because average altered basaltic crust has La/Pr value of 1.65 (Kelley et al., 2003), whereas the upper continental crust has a value of 4.37 (Rudnick & Gao, 2003). Therefore, lower La/Pr ratios are indicative of an increased basaltic input, either from basalt–seawater interaction or re-oxygenation of seafloor sediment. La/Pr ratios decrease at the beginning of the OAE level and during the interval of the two cooling events, particularly the main PCE, at which level it is consistent with positive shifts in Nd isotopes.

Re-oxygenation of bottom water has also been invoked as the cause of decreased TOC in Plenus records from the Tethys, North Atlantic, and even Japan (Bowman & Bralower, 2005; Dickson et al., 2016; Eldrett et al., 2014, 2017; Forster et al., 2007; Jarvis et al., 2011; Kuhnt et al., 2017; Nemoto & Hasegawa, 2011; Sinninghe Damsté et al., 2010; Tsikos et al., 2004; van Helmond et al., 2013, 2014). However, many sites record no change in the TOC, or in some cases an increase, suggesting locally sustained bottom-water oxygenation or simply changes in productivity (e.g., Dickson et al., 2016; Gavrilov et al., 2013; Kolonic et al., 2005; Kuhnt et al., 2017; Kuypers et al., 2002; Mort et al., 2007; Tsikos et al., 2004).

Faunal records showing an increase in benthic organisms and bioturbation during the Plenus interval suggest increased bottom-water oxygenation at sites across the Chalk Sea of northern Europe (Jarvis et al., 1988; Paul et al., 1999; Peryt & Lamolda, 1996; Takashima et al., 2009), Tethyan margin (Barroso-Barcenilla et al., 2011; Kalanat et al., 2016), North Atlantic (Eldrett et al., 2017), and Western Interior Seaway (Desmares et al., 2007; Elderbak et al., 2014). However, as with the TOC records, some sites show no change in benthic faunal abundance over this interval, or in some cases a decrease, further suggesting locally sustained bottom-water anoxia (e.g., El-Sabbagh et al., 2011; Friedrich et al., 2006; Grosheny et al., 2006, 2017; Keller et al., 2008).

Trace-metal, isotope, TOC, and faunal records all suggest pockets of re-oxygenation, but it remains difficult to link these directly to global changes in the carbon cycle or temperature. Furthermore, different water depths at different sites will have directly influenced bottom-water oxygenation, and may determine whether anoxia could have occurred in the first place.

5. Implications for Understanding Environmental Changes During the Plenus Cold Event

5.1. Carbon-Cycle Perturbation

The remarkable consistency of the carbon-isotope signature of OAE 2 across the globe allows for chemostratigraphic correlation of the event, albeit with the caveat that variable organic-matter sources can affect bulk $\delta^{13}\text{C}_{\text{org}}$ and variable diagenesis can affect $\delta^{13}\text{C}_{\text{carb}}$, particularly in sediments containing potentially reactive organic matter.

In a comparison of biostratigraphy and chemostratigraphy of OAE 2 between Europe and North America, Gale et al. (1993) found a consistent relationship between the two, which these authors took as evidence for effective synchronicity between certain paleontological markers and the carbon-isotope events in Europe and North America (despite some endemism and preservation problems, particularly associated with facies changes). More recent and higher-resolution studies support this contention, namely, global parallels in the general patterns of microfossil and macrofossil biostratigraphy and $\delta^{13}\text{C}$ correlations (Jarvis et al., 2006; Wendler, 2013). These records indicate a globally synchronous response of the biostratigraphic and chemostratigraphic record to the OAE, and that the characteristic carbon-isotope signature can be reliably used in correlation.

The terrestrially derived CO_2 records and the majority of marine CO_2 records show a rise then fall in atmospheric CO_2 across the P-CIE, suggesting a global carbon-cycle event. As such, we propose that the negative $\delta^{13}\text{C}$ excursion could—and should—be used as a stratigraphic marker to identify the Plenus interval in local archives. This approach to stratigraphic correlation avoids potential miscorrelation issues caused by possible diachroneity of any cooling observed at different locations, which could have been impacted by the local oceanographic conditions.

The driver of this CO_2 change is more difficult to identify. Initially, it was proposed that increased organic-carbon burial during the initial stages of OAE 2 drove a drawdown of atmospheric CO_2 (Arthur et al., 1988; Forster et al., 2007; Freeman & Hayes, 1992; Jarvis et al., 2011; Jenkyns et al., 1994; Kuypers et al., 1999; Sinninghe Damsté et al., 2010). Therefore, an increase in bottom-water re-oxygenation during the Plenus interval would have led to a temporary reduction of organic-matter deposition and/or the remineralization of sedimentary carbon on the sea floor, driving an increase in CO_2 . The Cenomanian–Turonian boundary was also a period of enhanced basalt–seawater interaction owing to the emplacement of at least two large igneous provinces (LIPs): the Caribbean Large Igneous Province (CLIP; Snow et al., 2005) and the High Arctic Large Igneous Province (HALIP; Tegner et al., 2011; Davis et al., 2016; Kingsbury et al., 2018; Schröder-Adams et al., 2019). A cessation of this volcanic outgassing may have resulted in an overall decrease in $p\text{CO}_2$ (e.g., Du Vivier et al., 2014, 2015; Scaife et al., 2017; Turgeon & Creaser, 2008). Indeed, Kuroda et al. (2007) suggested, based on a coeval shift in Pb isotopes indicative of an increase in hydrothermal input of Pb, that the negative carbon-isotope excursion observed during the Plenus interval reflects an increase in $p\text{CO}_2$ due to volcanism, rather than a drop in global burial rates of organic carbon. The changing balance between CO_2 drawdown due to organic-carbon burial versus volcanic and tectonic emissions of this greenhouse gas is difficult to constrain. However, a rise in atmospheric CO_2 would drive an increase in global temperatures—the opposite of what is observed. This apparent mismatch between theory and observation highlights complications in drawing causative links between putative CO_2 levels and the PCE, as it was originally interpreted.

5.2. Accompanying Climatic Phenomena

There is a wealth of data indicating widespread paleoenvironmental change during the early stages of OAE 2 but the question remains as to what drove such phenomena in different parts of the globe. Accounting for problems inherent in biostratigraphic, chemostratigraphic, and lithostratigraphic correlation, the records show little consistency in the timing of temperature and seawater chemistry (Figures 5 and 7). The onset

of these changes apparently appeared much earlier at some sites than others, even locally preceding the negative carbon-isotope excursion, suggesting that oceanic processes may have responded to forcing mechanisms other than just changes in ocean–atmosphere $p\text{CO}_2$, such as a change in local circulation, productivity, or basalt–seawater interactions.

5.2.1. Changing Water Mass Character

A change in circulation, bottom-water re-oxygenation, and basalt–seawater interactions have variously been proposed to drive the excursions seen in different proxy records discussed in section 4.3. However, records of seawater chemistry are difficult to interpret as the proxies may have responded to more than one process, or one process may have driven another. The neodymium-isotopic signal of a water mass may reflect changes in circulation, but it can also be affected by basalt–seawater interaction introducing radiogenic Nd. Although complicating the interpretation of ϵ_{Nd} records, the geochemical imprint of basalt on seawater may be helpful for tracing the source of a water mass to volcanically affected areas.

The positive ϵ_{Nd} excursion in the Eastbourne record was interpreted by Zheng et al. (2016) to reflect the input of strongly radiogenic Nd from volcanism through relatively oxygen-poor water, citing the coeval emplacement of the Caribbean Large Igneous Province (Snow et al., 2005) and the High Arctic Large Igneous Province (Davis et al., 2016; Kingsbury et al., 2018; Tegner et al., 2011). Due to the lack of outcrop, the chemistry and eruption history of these LIPs are poorly constrained, which makes it difficult to pinpoint the source of any volcanically derived radiogenic Nd. For CLIP to have acted as the source of radiogenic Nd would have required transfer of the geochemical bottom-water signal from the Pacific Ocean to southern England across the eastern paleo-Pacific and proto-Atlantic (cf. Trabucho-Alexandre, 2014). Given that the residence time of neodymium in the ocean today is roughly equal to the mixing time of the ocean (Frank, 2002; Goldstein & Hemming, 2003; Thomas, 2005), CLIP-derived radiogenic Nd is unlikely to have induced such a large positive shift in ϵ_{Nd} in such a distal location as southern England. Neodymium might have had a longer residence time in relatively deoxygenated seawater because Fe-Mn oxyhydroxides (a sink for Nd) would not have been stable under such conditions (Halliday et al., 1992); however, such conditions would have been less applicable during the apparently more oxygenated conditions (at least in southern England) of the PCE itself. If a water mass from the vicinity of the HALIP moved south, carrying a radiogenic Nd signature, it could have produced a positive ϵ_{Nd} excursion while simultaneously causing a drop in water temperature, as seen in the Dover record (Figure 2). Furthermore, as O_2 solubility is dependent on water temperature (e.g., Broecker & Peng, 1974), a cold water mass would have contained higher concentrations of dissolved O_2 compared with warmer waters and could have induced a redox shift in bottom waters, as suggested by the trace-metal record at Dover (Figure 2) and Eastbourne (Jenkyns et al., 2017).

Trace-metal and isotopic excursions have been ascribed to two factors: (1) bottom-water re-oxygenation during the PCE, whereby the remineralization of trace-metal-rich organic matter deposited during the early stages of the OAE released metals into the water column, some of which were subsequently incorporated into nannofossil and foraminiferal carbonate (Jenkyns et al., 2017), and (2) alternatively, or additionally, the transient loss of the organic-rich sink during re-oxygenation events during the Plenus interval, with ongoing basalt–seawater interaction continuing to liberate volcanically derived trace metals, allowed their buildup in ocean waters (Orth et al., 1993; Pearce et al., 2009; Holmden et al., 2016; Jenkyns et al., 2017).

Decreased TOC across the Plenus interval has also been suggested to indicate a redox shift (e.g., Eldrett et al., 2014, 2017; Jarvis et al., 2011; Tsikos et al., 2004), although organic-matter content may be affected by changes in preservation, productivity, or dilution. Increased oxygenation of bottom waters would inhibit the deposition of organic matter, although this assumes a simple coupling between anoxia and organic-matter deposition in the first place, which is manifestly a gross simplification (e.g., Demaison & Moore, 1980; Pedersen & Calvert, 1990). Deposition of the characteristic black shales of OAE 2 was not a global phenomenon, but rather limited to environments that favorably supported organic-matter burial, particularly the Atlantic and Tethyan regions and the equatorial Pacific (Schlanger et al., 1987; Takashima et al., 2009). Furthermore, local to regional variations in productivity, preservation, sedimentation rate, and seawater chemistry led to differences in the timing of local maxima in organic-carbon burial rates. Particularly in former upwelling areas, such as the western sides of continents or the paleo-equator, increases in organic productivity, initially unrelated to bottom-water or midwater redox, may have driven

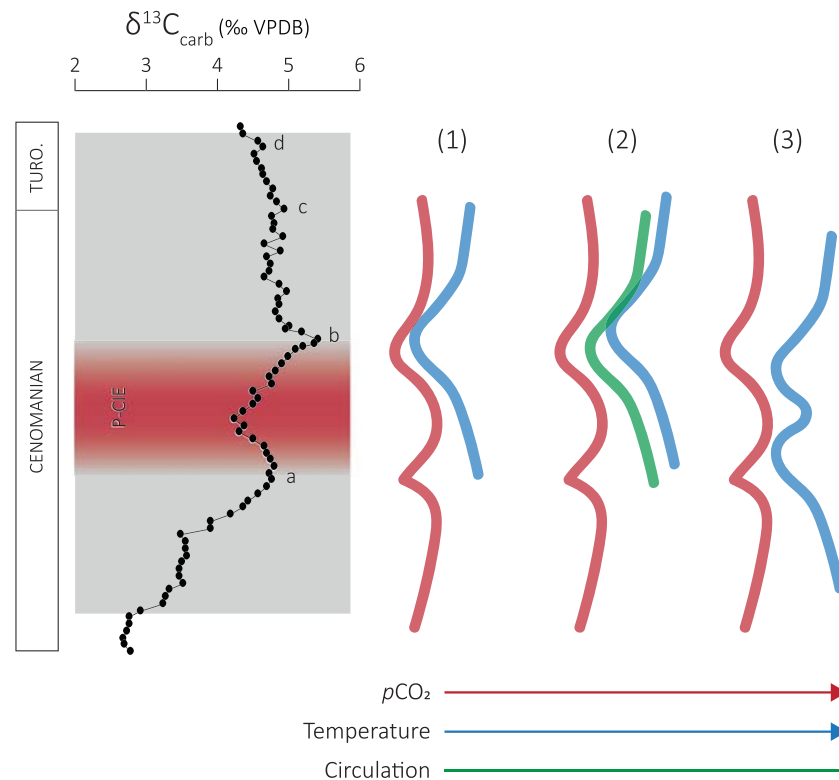


Figure 9. Potential models for cooling during the PCE. $\delta^{13}\text{C}$ from Eastbourne (Tsikos et al., 2004). The gray box indicates the OAE 2 interval and the red band indicates the P-CIE; points “a” to “d” of the $\delta^{13}\text{C}$ curve are labeled. The red lines indicate CO_2 , the blue lines indicate SST, and the green line indicates circulation. Values are arbitrary. Model (1): A direct link between CO_2 , atmospheric temperatures, and SSTs would produce a cooling interval after a drop in CO_2 . Model (2): A fall in CO_2 would drive global temperature decrease, forcing a circulation change and, in turn, further cooling. In this model, cooling must come after the CO_2 change. Model (3): No direct link between CO_2 and SSTs would produce variable timing and expression of temperatures at individual sites.

an increase in organic-matter deposition. An increased supply of biologically significant metals or minerals may also have resulted directly from basalt–seawater interactions, and/or increased terrestrial weathering, and consequent accelerated fluvial nutrient input to the oceans, which may in turn have driven an expansion of organic productivity (Jenkyns, 2010). Local changes in these processes—whether related or unrelated to global CO_2 and temperature—may have driven either an increase or decrease in organic-matter deposition that might be misconstrued as a redox shift. These factors may also explain the records of increased TOC across the Plenius interval in Spain (Mort et al., 2007) and Morocco (Kuhnt et al., 2017). Given the enhanced hydrological cycle, proposed to have driven an increase in silicate weathering during the OAE (Blättler et al., 2011; Pogge von Strandmann et al., 2013), changes in terrestrial weathering and sedimentary dilution may also have affected the TOC without changing productivity or preservation.

5.2.2. Cooling

Cooling events are observed across the Northern Hemisphere during the Plenius interval, for which a range of mechanisms has been proposed.

1. A causal link has been suggested between SSTs and the carbon cycle during OAE 2: at its simplest, the widespread deposition of organic matter during OAE 2 is credited with leading to CO_2 drawdown and, in turn, transient cooling (Arthur et al., 1988; Forster et al., 2007; Freeman & Hayes, 1992; Jarvis et al., 2011; Jenkyns et al., 1994; Kuypers et al., 1999; Sinninghe Damsté et al., 2010). However, if these temperature records (TEX_{86} , $\delta^{18}\text{O}$, fauna) were solely recording the SST response to global atmospheric cooling, they would be expected to show a degree of synchronicity and expression: cooling occurring *during and after* the CO_2 decrease, during the later phase of the P-CIE close to point “b” (e.g., scenario (1) in

- Figure 9; Eastbourne and ODP Site 1276 in Figure 7). While a global decrease in temperatures would have been a necessary response to falling atmospheric CO₂ levels, the SST records—if accepted at face value—show significant variability in the timing of the cooling relative to the P-CIE. The TEX₈₆, δ¹⁸O, and faunal records that show cooling preceding the CO₂ decrease, in the early phase of the P-CIE close to point “a” (e.g., Wunstorf, Gröbern, Bass River, Pueblo; Figure 7), which implies either an indirect response of local SSTs to CO₂ change, or simply the effect of local oceanographic conditions independent of global change. Furthermore, it is difficult to directly link the cooling seen at point “b” to global processes, when the drop in temperature may have been due to a circulation change bringing cooler water to a locality (as seen by the simultaneous cooling and Nd excursion in SE England; Figures 2 and 9).
2. Ocean circulation is thought to have been a critical component of the climate system during the Plenus interval, wherein CO₂ drawdown led to global cooling and increased latitudinal temperature gradients, which in turn drove a change in circulation (Eldrett et al., 2017; van Helmond et al., 2014; Zheng et al., 2013). However, there are two problems with this hypothesis. Firstly, as in (1), this model does not account for cooling preceding the CO₂ decrease. Secondly, if global cooling drove the circulation change, one would expect one phase of cooling after the CO₂ change then another after the circulation change, but none of the records show this. As such, this model cannot account for cooling in the early phase of the P-CIE, close to point “a,” which indicates that CO₂-driven circulation change was not a direct driver of the cooling at all sites.
 3. Alternatively, circulation might have been altered due to factors unrelated to global temperatures and latitudinal gradients, perhaps owing to changes in upwelling (e.g., Einsele & Wiedmann, 1982; Kolonic et al., 2005), deepening and shallowing of local sea levels affecting upper ocean circulation patterns (e.g., Hancock, 1993; Voigt & Wiese, 2000; Voigt et al., 2006), or LIP-related tectonics (e.g., Dostal & MacRae, 2018; Maher, 2001). These changes in circulation may have brought cooler water masses to regions bordering the Arctic, producing a decrease in local SSTs. Within the Chalk Sea and the Western Interior Seaway, rises in δ¹³C correlate with local transgressions (Voigt & Hillbrecht, 1997; Voigt & Wiese, 2000; Laurin et al., 2019). The timing of the cooling and circulation change observed in the Chalk Sea of southern England is coincident with the rising limb of the P-CIE and evidence for a local transgression, suggesting that deepening of the sea may have allowed an ingress of cooler boreal waters.

Although OAE 2 was a period of extreme global climate perturbation, the local temperature responses to increased CO₂ likely varied in magnitude, trend and, potentially, sign. Thus, interactions between climatic and oceanographic processes may account for the different expressions of cooling seen at different sites, especially the cooling seen in the early stages of the P-CIE. If nothing else, the apparent diachroneity in cooling highlights the problems associated with using any local expression of temperature or water mass character during the Plenus interval as a correlation tool or stratigraphic marker.

6. Conclusions

The Cenomanian–Turonian transition experienced extreme climate change and major volcanic and tectonic activity. The increase in silicate weathering due to an enhanced hydrological cycle on the continents and the weathering of LIP-related basalts in the oceans probably drove a drawdown in CO₂, as did high rates of organic-carbon burial. The ongoing basalt–seawater interaction, likely concentrated in the first half of OAE 2 based on regional osmium-isotope signatures (Du Vivier et al., 2014, 2015), would have further affected both atmospheric pCO₂ and global carbon-isotope compositions. By contrast, volcanic outgassing and the cessation of organic-carbon deposition would have driven an *increase* in pCO₂. However, it is not possible to disentangle these processes and their effects on the carbon cycle from the current data.

During the Plenus interval, there is evidence for widespread environmental change across the Northern Hemisphere. The global extent of negative δ¹³C excursions, coincident with records of increasing pCO₂, suggest an increase in atmospheric CO₂ and a global carbon-cycle event—the Plenus CIE. However, the records of cooling show no consistency in timing or expression, and suggest either that some or all of the proxy records are compromised by diagenesis or environmental factors, and/or there was no clear-cut link between SSTs and atmospheric pCO₂. While there was likely a global fall in temperatures relating to the drop in CO₂, applying simple cause-and-effect relationships between CO₂ and temperature does not explain all observations. Furthermore, variability in the timing and expression of changes in seawater chemistry, and problems in

determining the driver of observed proxy changes, suggests that no one simple mechanism can link the carbon cycle to oceanography during the Plenus interval. While these stratigraphic offsets do not contradict the hypothesis of a global $p\text{CO}_2$ decrease directly driving cooling with a concomitant or subsequent change in ocean circulation, they do suggest that local effects played a modifying role on the local timing and expression of events. To advance the understanding of the Plenus event, more geographically widespread records are required, ideally with proxies for temperature, CO_2 , and ocean circulation applied in a single setting.

Given the global nature of the negative $\delta^{13}\text{C}$ excursion and the decrease in atmospheric $p\text{CO}_2$, it is proposed that the Plenus CIE is a more reliable stratigraphic marker to identify the stratigraphic interval during which local expressions of the Plenus interval were developed with or without evidence for a fall in temperature and/or a drop in $p\text{CO}_2$.

Acknowledgments

The authors would like to thank Alan Hseih, Chris Day, and Steve Wyatt for their technical assistance at the Department of Earth Sciences, University of Oxford. L.K.O. would like to thank the Clarendon Fund (University of Oxford) and University College, Oxford, for supporting her DPhil. S.R.C.R. would like to thank NERC GW4+ for his studentship. Data are available in the supporting information and at <https://doi.pangaea.de/10.1594/PANGAEA.909150>.

References

- Arthur, M. A., Brumsack, H.-J., Jenkyns, H. C., & Schlanger, S. O. (1990). Stratigraphy, Geochemistry, and Paleoceanography of Organic Carbon-Rich Cretaceous Sequences. In: R. N. Ginsburg & B. Beaudoin (Eds.), *Cretaceous Resources, Events and Rhythms, NATO ASI Series*, 304, 75–119. https://doi.org/10.1007/978-94-015-6861-6_6
- Arthur, M. A., Dean, W. E., & Pratt, L. M. (1988). Geochemical and climatic effects of increased marine organic carbon burial at the Cenomanian/Turonian boundary. *Nature*, 335(6192), 714–717. <https://doi.org/10.1038/335714a0>
- Barclay, R. S., McElwain, J. C., & Sageman, B. B. (2010). Carbon sequestration activated by a volcanic CO_2 pulse during ocean anoxic event 2. *Nature Geoscience*, 3(3), 205–208. <https://doi.org/10.1038/ngeo757>
- Barroso-Barcenilla, F., Pascual, A., Peyrot, D., & Rodríguez-Lázaro, J. (2011). Integrated biostratigraphy and chemostratigraphy of the upper Cenomanian and lower Turonian succession in Puentevedey, Iberian trough, Spain. *Proceedings of the Geologists' Association*, 122(1), 67–81. <https://doi.org/10.1016/j.pgeola.2010.11.002>
- Berger, W. H., & Vincent, E. (1986). Deep-sea carbonates: Reading the carbon-isotope signal. *Geologische Rundschau*, 75(1), 249–269. <https://doi.org/10.1007/bf01770192>
- Blättler, C. L., Jenkyns, H. C., Reynard, L. M., & Henderson, G. M. (2011). Significant increases in global weathering during oceanic anoxic events 1a and 2 indicated by calcium isotopes. *Earth and Planetary Science Letters*, 309(1–2), 77–88. <https://doi.org/10.1016/j.epsl.2011.06.029>
- Bomou, B., Adatte, T., Tantawy, A. A., Mort, H., Fleitmann, D., Huang, Y., & Föllmi, K. B. (2013). The expression of the Cenomanian–Turonian oceanic anoxic event in Tibet. *Paleogeography, Paleoclimatology, Paleoecology*, 369, 466–481. <https://doi.org/10.1016/j.paleo.2012.11.011>
- Bonnand, P., James, R. H., Parkinson, I. J., Connelly, D. P., & Fairchild, I. J. (2013). The chromium isotopic composition of seawater and marine carbonates. *Earth and Planetary Science Letters*, 382, 10–20. <https://doi.org/10.1016/j.epsl.2013.09.001>
- Bowman, A. R., & Bralower, T. J. (2005). Paleoclimatographic significance of high-resolution carbon isotope records across the Cenomanian–Turonian boundary in the Western Interior and New Jersey coastal plain, USA. *Marine Geology*, 217(3–4), 305–321. <https://doi.org/10.1016/j.margeo.2005.02.010>
- Broecker, W. S., & Peng, T.-H. (1974). Gas exchange rates between air and sea. *Tellus*, 26(5), 21–35. <https://doi.org/10.3402/tellusa.v26i5.9869>
- Caron, M., Dall'Agnolo, S., Accarie, H., Barrera, E., Kauffman, E. G., Amédéo, F., & Robaszynski, F. (2006). High-resolution stratigraphy of the Cenomanian–Turonian boundary interval at Pueblo (USA) and Wadi Bahloul (Tunisia): Stable isotope and bio-events correlation. *Geobios*, 39(2), 171–200. <https://doi.org/10.1016/j.geobios.2004.11.004>
- Charbonnier, G., Adatte, T., Spangenberg, J. E., & Föllmi, K. B. (2018). The expression of early Aptian to latest Cenomanian oceanic anoxic events in the sedimentary record of the Briançonnais domain. *Global and Planetary Change*, 170, 76–92. <https://doi.org/10.1016/j.gloplacha.2018.08.009>
- Clarkson, M. O., Stirling, C. H., Jenkyns, H. C., Dickson, A. J., Porcelli, D., Moy, C. M., et al. (2018). Uranium isotope evidence for two episodes of deoxygenation during oceanic anoxic event 2. *Proceedings of the National Academy of Sciences*, 115(12), 2918–2923. <https://doi.org/10.1073/pnas.1715278115>
- Corfield, R. M., Hall, M. A., & Brasier, M. D. (1990). Stable isotope evidence for foraminiferal habitats during the development of the Cenomanian/Turonian oceanic anoxic event. *Geology*, 18(2), 175–178. [https://doi.org/10.1130/0091-7613\(1990\)018<0175:SIEFFH>2.3.CO;2](https://doi.org/10.1130/0091-7613(1990)018<0175:SIEFFH>2.3.CO;2)
- Danzelle, J., Riquier, L., Baudin, F., Thomazo, C., & Pucéat, E. (2018). Oscillating redox conditions in the Vocontian Basin (SE France) during oceanic anoxic event 2 (OAE 2). *Chemical Geology*, 493, 136–152. <https://doi.org/10.1016/j.chemgeo.2018.05.039>
- Davis, W. J., Schröder-Adams, C. J., Galloway, J. M., Herrie, J. O., & Pugh, A. T. (2016). U–Pb geochronology of bentonites from the Upper Cretaceous Kanguk Formation, Sverdrup Basin, Arctic Canada: Constraints on sedimentation rates, biostratigraphic correlations and the late magmatic history of the High Arctic Large Igneous Province. *Geological Magazine*, 154(04), 757–776. <https://doi.org/10.1017/s0016756816000376>
- De Baar, H. J., German, C. R., Elderfield, H., & van Gaans, P. (1988). Rare earth element distributions in anoxic waters of the Cariaco Trench. *Geochimica et Cosmochimica Acta*, 52(5), 1203–1219. [https://doi.org/10.1016/0016-7037\(88\)90275-x](https://doi.org/10.1016/0016-7037(88)90275-x)
- Demaison, G. J., & Moore, G. T. (1980). Anoxic environments and oil source bed genesis. *Organic Geochemistry*, 2(1), 9–31. [https://doi.org/10.1016/0146-6380\(80\)90017-0](https://doi.org/10.1016/0146-6380(80)90017-0)
- Desmares, D., Crognier, N., Bardin, J., Testé, M., Beaudoin, B., & Grosheny, D. (2016). A new proxy for Cretaceous paleoceanographic and paleoclimatic reconstructions: Coiling direction changes in the planktonic foraminifera *Muricohedbergella delrioensis*. *Paleogeography, Paleoclimatology, Paleoecology*, 445, 8–17. <https://doi.org/10.1016/j.paleo.2015.12.021>
- Desmares, D., Grosheny, D., Beaudoin, B., Gardin, S., & Gauthier-Lafaye, F. (2007). High resolution stratigraphic record constrained by volcanic ash beds at the Cenomanian–Turonian boundary in the Western Interior Basin, USA. *Cretaceous Research*, 28(4), 561–582. <https://doi.org/10.1016/j.cretres.2006.08.009>

- Dickson, A. J., Jenkyns, H. C., Porcelli, D., van den Boorn, S., & Idiz, E. (2016). Basin-scale controls on the molybdenum-isotope composition of seawater during Oceanic Anoxic Event 2 (Late Cretaceous). *Geochimica et Cosmochimica Acta*, *178*, 291–306. <https://doi.org/10.1016/j.gca.2015.12.036>
- Dickson, A. J., Saker-Clark, M., Jenkyns, H. C., Bottini, C., Erba, E., Russo, F., et al. (2017). A southern hemisphere record of global trace-metal drawdown and orbital modulation of organic-matter burial across the Cenomanian–Turonian boundary (Ocean Drilling Program Site 1138, Kerguelen plateau). *Sedimentology*, *64*(1), 186–203. <https://doi.org/10.1111/sed.12303>
- Dostal, J., & MacRae, A. (2018). Cretaceous basalts of the High Arctic large igneous province at Axel Heiberg Island (Canada): Volcanic stratigraphy, geodynamic setting, and origin. *Geological Journal*, *53*(6), 2918–2934. <https://doi.org/10.1002/gj.3132>
- Du Vivier, A. D. C., Selby, D., Condon, D. J., Takashima, R., & Nishi, H. (2015). Pacific $^{187}\text{Os}/^{188}\text{Os}$ isotope chemistry and U–Pb geochronology: Synchronicity of global Os isotope change across OAE 2. *Earth and Planetary Science Letters*, *428*, 204–216. <https://doi.org/10.1016/j.epsl.2015.07.020>
- Du Vivier, A. D. C., Selby, D., Sageman, B. B., Jarvis, I., Gröcke, D. R., & Voigt, S. (2014). Marine $^{187}\text{Os}/^{188}\text{Os}$ isotope stratigraphy reveals the interaction of volcanism and ocean circulation during Oceanic Anoxic Event 2. *Earth and Planetary Science Letters*, *389*, 23–33. <https://doi.org/10.1016/j.epsl.2013.12.024>
- Eicher, D. L., & Diner, R. (1985). Foraminifera as indicators of water mass in the Cretaceous Greenhorn Sea, Western Interior. In L. M. Pratt, E. G. Kauffman, & F. B. Zelt (Eds.), *Fine-grained deposits and biofacies of the Cretaceous Western Interior Seaway: Evidence of cyclic sedimentary processes, Fieldtrip Guidebook* (Vol 4) (pp. 60–71). Tulsa, Oklahoma: Society of Economic Paleontologists and Mineralogists. <https://doi.org/10.2110/sepmfg.04.060>
- Eicher, D. L., & Worstell, P. (1970). Cenomanian and Turonian foraminifera from the Great Plains, United States. *Micropaleontology*, *16*(3), 269. <https://doi.org/10.2307/1485079>
- Einsele, G., & Wiedmann, J. (1982). Turonian black shales in the Moroccan coastal basins: First upwelling in the Atlantic Ocean? *Geology of the Northwest African Continental Margin*, 396–414. https://doi.org/10.1007/978-3-642-68409-8_16
- Eldrett, J. S., Dodsworth, P., Bergman, S. C., Wright, M., & Minisini, D. (2017). Water-mass evolution in the Cretaceous Western Interior Seaway of North America and equatorial Atlantic. *Climate of the Past*, *13*(7), 855–878. <https://doi.org/10.5194/cp-13-855-2017>
- Eldrett, J. S., Minisini, D., & Bergman, S. C. (2014). Decoupling of the carbon cycle during Ocean Anoxic Event 2. *Geology*, *42*(7), 567–570. <https://doi.org/10.1130/g35520.1>
- Elrick, M., Molina-Garza, R., Duncan, R., & Snow, L. (2009). C-isotope stratigraphy and paleoenvironmental changes across OAE2 (mid-Cretaceous) from shallow-water platform carbonates of southern Mexico. *Earth and Planetary Science Letters*, *277*(3–4), 295–306. <https://doi.org/10.1016/j.epsl.2008.10.020>
- El-Sabbagh, A., Tantawy, A. A., Keller, G., Khozyem, H., Spangenberg, J., Adatte, T., & Gertsch, B. (2011). Stratigraphy of the Cenomanian–Turonian Oceanic Anoxic Event OAE2 in shallow shelf sequences of NE Egypt. *Cretaceous Research*, *32*(6), 705–722. <https://doi.org/10.1016/j.cretres.2011.04.006>
- Erbacher, J., Friedrich, O., Wilson, P. A., Birch, H., & Mutterlose, J. (2005). Stable organic carbon isotope stratigraphy across Oceanic Anoxic Event 2 of Demerara Rise, western tropical Atlantic. *Geochemistry, Geophysics, Geosystems*, *6*(6). <https://doi.org/10.1029/2004gc000850>
- Farouk, S., Ahmad, F., & Powell, J. H. (2017). Cenomanian–Turonian stable isotope signatures and depositional sequences in Northeast Egypt and Central Jordan. *Journal of Asian Earth Sciences*, *134*, 207–230. <https://doi.org/10.1016/j.jseaes.2016.11.021>
- Farquhar, G. D., Ehleringer, J. R., & Hubick, K. T. (1989). Carbon isotope discrimination and photosynthesis. *Annual Review of Plant Biology*, *40*(1), 503–537. <https://doi.org/10.1146/annurev.pp.40.060189.002443>
- Fisher, J. K., Price, G. D., Hart, M. B., & Leng, M. J. (2005). Stable isotope analysis of the Cenomanian–Turonian (Late Cretaceous) oceanic anoxic event in the Crimea. *Cretaceous Research*, *26*(6), 853–863. <https://doi.org/10.1016/j.cretres.2005.05.010>
- Forster, A., Kuypers, M. M. M., Turgeon, S. C., Brumsack, H.-J., Petrizzo, M. R., & Sinninghe Damsté, J. S. (2008). The Cenomanian/Turonian oceanic anoxic event in the South Atlantic: New insights from a geochemical study of DSDP Site 530A. *Paleogeography, Paleoclimatology, Paleocology*, *267*(3–4), 256–283. <https://doi.org/10.1016/j.paleo.2008.07.006>
- Forster, A., Schouten, S., Moriya, K., Wilson, P. A., & Sinninghe Damsté, J. S. (2007). Tropical warming and intermittent cooling during the Cenomanian/Turonian oceanic anoxic event 2: Sea surface temperature records from the equatorial Atlantic. *Paleoceanography*, *22*(1), PA1219. <https://doi.org/10.1029/2006pa001349>
- Frank, M. (2002). Radiogenic isotopes: Tracers of past ocean circulation and erosional input. *Reviews of Geophysics*, *40*(1), 1–38. <https://doi.org/10.1029/2000rg000094>
- Freeman, K. H., & Hayes, J. M. (1992). Fractionation of carbon isotopes by phytoplankton and estimates of ancient CO₂ levels. *Global Biogeochemical Cycles*, *6*(2), 185–198. <https://doi.org/10.1029/92gb00190>
- Friedrich, O., Erbacher, J., & Mutterlose, J. (2006). Paleoenvironmental changes across the Cenomanian/Turonian boundary event (Oceanic Anoxic Event 2) as indicated by benthic foraminifera from the Demerara Rise (ODP Leg 207). *Revue de Micropaleontologie*, *49*(3), 121–139. <https://doi.org/10.1016/j.revmic.2006.04.003>
- Gale, A. S., & Christensen, W. K. (1996). Occurrence of the belemnite *Actinocamax plenus* in the Cenomanian of SE France and its significance. *Bulletin of the Geological Society of Denmark*, *43*(1), 68–77.
- Gale, A. S., Jenkyns, H. C., Kennedy, W. J., & Corfield, R. M. (1993). Chemostratigraphy versus biostratigraphy: Data from around the Cenomanian–Turonian boundary. *Journal of the Geological Society*, *150*(1), 29–32. <https://doi.org/10.1144/gsjgs.150.1.0029>
- Gale, A. S., Jenkyns, H. C., Tsikos, H., van Breugel, Y., Sinninghe Damsté, J. S., Bottini, C., et al. (2019). High-resolution bio- and chemostratigraphy of an expanded record of Oceanic Anoxic Event 2 (Late Cenomanian–Early Turonian) at Clot Chevalier, near Barrême, SE France (Vocontian Basin). *Newsletters on Stratigraphy*, *52*(1), 97–129. <https://doi.org/10.1127/nos/2018/0445>
- Gale, A. S., Kennedy, W. J., Voigt, S., & Walaszczyk, I. (2005). Stratigraphy of the upper Cenomanian–lower Turonian chalk succession at Eastbourne, Sussex, UK: Ammonites, inoceramid bivalves and stable carbon isotopes. *Cretaceous Research*, *26*(3), 460–487. <https://doi.org/10.1016/j.cretres.2005.01.006>
- Gangl, S. K., Moy, C. M., Stirling, C. H., Jenkyns, H. C., Crampton, J. S., Clarkson, M. O., et al. (2019). High-resolution records of Oceanic Anoxic Event 2: Insights into the timing, duration and extent of environmental perturbations from the palaeo-South Pacific Ocean. *Earth and Planetary Science Letters*, *518*, 172–182. <https://doi.org/10.1016/j.epsl.2019.04.028>
- Gavrilov, Y. O., Shcherbinina, E. A., Golovanova, O. V., & Pokrovskii, B. G. (2013). The late Cenomanian paleoecological event (OAE 2) in the eastern Caucasus basin of northern Peri-Tethys. *Lithology and Mineral Resources*, *48*(6), 457–488. <https://doi.org/10.1134/s0024490213060047>
- Goldstein, S. L., & Hemming, S. R. (2003). Long-lived isotopic tracers in oceanography, paleoceanography, and ice-sheet dynamics. *Treatise on Geochemistry*, 453–489. <https://doi.org/10.1016/b0-08-043751-6/06179-x>

- Grosheny, D., Beaudoin, B., Morel, L., & Desmares, D. (2006). High-resolution biostratigraphy and chemostratigraphy of the Cenomanian/Turonian boundary event in the Vocontian Basin, Southeast France. *Cretaceous Research*, 27(5), 629–640. <https://doi.org/10.1016/j.cretres.2006.03.005>
- Grosheny, D., Ferry, S., Lécuyer, C., Thomas, A., & Desmares, D. (2017). The Cenomanian–Turonian boundary event (CTBE) on the southern slope of the Subalpine Basin (SE France) and its bearing on a probable tectonic pulse on a larger scale. *Cretaceous Research*, 72, 39–65. <https://doi.org/10.1016/j.cretres.2016.11.009>
- Halliday, A. N., Davidson, J. P., Holden, P., Owen, R. M., & Olivarez, A. M. (1992). Metalliferous sediments and the scavenging residence time of Nd near hydrothermal vents. *Geophysical Research Letters*, 19(8), 761–764. <https://doi.org/10.1029/92gl00393>
- Hancock, J. M. (1975). The petrology of the Chalk. *Proceedings of the Geologists' Association*, 86(4), 499–535. [https://doi.org/10.1016/s0016-7878\(75\)80061-7](https://doi.org/10.1016/s0016-7878(75)80061-7)
- Hancock, J. M. (1993). Sea-level changes around the Cenomanian–Turonian boundary. *Cretaceous Research*, 14(4–5), 553–562. <https://doi.org/10.1006/cres.1993.1039>
- Hancock, J. M., & Kauffman, E. G. (1979). The great transgressions of the Late Cretaceous. *Journal of the Geological Society*, 136(2), 175–186. <https://doi.org/10.1144/gsjgs.136.2.0175>
- Hasegawa, T., Crampton, J. S., Schiøler, P., Field, B., Fukushi, K., & Kakizaki, Y. (2013). Carbon isotope stratigraphy and depositional oxia through Cenomanian/Turonian boundary sequences (Upper Cretaceous) in New Zealand. *Cretaceous Research*, 40, 61–80. <https://doi.org/10.1016/j.cretres.2012.05.008>
- Heimhofer, U., Wucherpfennig, N., Adatte, T., Schouten, S., Schneebeli-Hermann, E., Gardin, S., et al. (2018). Vegetation response to exceptional global warmth during Oceanic Anoxic Event 2. *Nature Communications*, 9(1), 3832. <https://doi.org/10.1038/s41467-018-06319-6>
- Holmden, C., Jacobson, A. D., Sageman, B. B., & Hurtgen, M. T. (2016). Response of the Cr isotope proxy to Cretaceous Ocean Anoxic Event 2 in a pelagic carbonate succession from the Western Interior Seaway. *Geochimica et Cosmochimica Acta*, 186, 277–295. <https://doi.org/10.1016/j.gca.2016.04.039>
- Jarvis, I., Carson, G. A., Cooper, M. K. E., Hart, M. B., Leary, P. N., Tocher, B. A., et al. (1988). Microfossil assemblages and the Cenomanian–Turonian (Late Cretaceous) Oceanic Anoxic Event. *Cretaceous Research*, 9, 3–103. [https://doi.org/10.1016/0195-6671\(88\)90003-1](https://doi.org/10.1016/0195-6671(88)90003-1)
- Jarvis, I., Gale, A. S., Jenkyns, H. C., & Pearce, M. A. (2006). Secular variation in Late Cretaceous carbon isotopes: A new $\delta^{13}\text{C}$ carbonate reference curve for the Cenomanian–Campanian (99.6–70.6 ma). *Geological Magazine*, 143(5), 561–608. <https://doi.org/10.1017/s0016756806002421>
- Jarvis, I., Lignum, J. S., Gröcke, D. R., Jenkyns, H. C., & Pearce, M. A. (2011). Black shale deposition, atmospheric CO_2 drawdown, and cooling during the Cenomanian–Turonian Oceanic Anoxic Event. *Paleoceanography*, 26(3), PA3201. <https://doi.org/10.1029/2010pa002081>
- Jarvis, I., Murphy, A. M., & Gale, A. S. (2001). Geochemistry of pelagic and hemipelagic carbonates: Criteria for identifying systems tracts and sea-level change. *Journal of the Geological Society of London*, 158, 685–696. <https://doi.org/10.1144/jgs.158.4.685>
- Jans, C. V., Long, D., Hall, M. A., Bland, D. J., & Cornford, C. (1991). The geochemistry of the Plenus Marls at Dover, England: Evidence of fluctuating oceanographic conditions and of glacial control during the development of the Cenomanian–Turonian $\delta^{13}\text{C}$ anomaly. *Geological Magazine*, 128(06), 603–632. <https://doi.org/10.1017/s0016756800019725>
- Jefferies, R. P. S. (1962). The palaeoecology of the *Actinocamax* Plenus Subzone (lowest Turonian) in the Anglo-Paris Basin. *Palaeontology*, 4(4), 609–647.
- Jefferies, R. P. S. (1963). The stratigraphy of the *Actinocamax plenus* Subzone (Turonian) in the Anglo-Paris Basin. *Proceedings of the Geologists' Association*, 74(1), 1–33. [https://doi.org/10.1016/s0016-7878\(63\)80011-5](https://doi.org/10.1016/s0016-7878(63)80011-5)
- Jenkyns, H. C. (2003). Evidence for rapid climate change in the Mesozoic–Paleogene greenhouse world. *Philosophical Transactions of the Royal Society, Series A: Mathematical, Physical and Engineering Sciences*, 361(1810), 1885–1916. <https://doi.org/10.1098/rsta.2003.1240>
- Jenkyns, H. C. (2010). Geochemistry of oceanic anoxic events. *Geochemistry, Geophysics, Geosystems*, 11(3), Q03004. <https://doi.org/10.1029/2009gc002788>
- Jenkyns, H. C. (2018). Transient cooling episodes during Cretaceous Oceanic Anoxic Events with special reference to OAE 1a (early Aptian). *Philosophical Transactions of the Royal Society, Series A: Mathematical, Physical and Engineering Sciences*, 376(2130), 20170073. <https://doi.org/10.1098/rsta.2017.0073>
- Jenkyns, H. C., Dickson, A. J., Ruhl, M., & van den Boorn, S. H. J. M. (2017). Basalt-seawater interaction, the Plenus Cold Event, enhanced weathering and geochemical change: Deconstructing Oceanic Anoxic Event 2 (Cenomanian–Turonian, Late Cretaceous). *Sedimentology*, 64(1), 16–43. <https://doi.org/10.1111/sed.12305>
- Jenkyns, H. C., Gale, A. S., & Corfield, R. M. (1994). Carbon- and oxygen-isotope stratigraphy of the English Chalk and Italian Scaglia and its palaeoclimatic significance. *Geological Magazine*, 131(01), 1–34. <https://doi.org/10.1017/s0016756800010451>
- Jones, M. M., Sageman, B. B., Oakes, R. L., Parker, A. L., Leckie, R. M., Bralower, T. J., et al. (2019). Astronomical pacing of relative sea level during Oceanic Anoxic Event 2: Preliminary studies of the expanded SH#1 Core, Utah, USA. *GSA Bulletin*. <https://doi.org/10.1130/b32057.1>
- Joo, Y. J., & Sageman, B. B. (2014). Cenomanian to Campanian carbon isotope chemostratigraphy from the Western Interior Basin, U.S.A. *Journal of Sedimentary Research*, 84(7), 529–542. <https://doi.org/10.2110/jsr.2014.38>
- Kaiho, K., Katabuchi, M., Oba, M., & Lamolda, M. (2014). Repeated anoxia-extinction episodes progressing from slope to shelf during the latest Cenomanian. *Gondwana Research*, 25(4), 1357–1368. <https://doi.org/10.1016/j.gr.2012.12.008>
- Kalanat, B., Gharaie, M. H. M., Vahidinia, M., & Matsumoto, R. (2018). Short-term eustatic sea-level changes during the Cenomanian–Turonian Supergreenhouse interval in the Kopet-Dagh Basin, NE Tethyan realm. *Journal of Iberian Geology*, 44(2), 177–191. <https://doi.org/10.1007/s41513-018-0060-8>
- Kalanat, B., Vahidinia, M., Vaziri-Moghaddam, H., & Mahmudy-Gharaie, M. H. (2016). Planktonic foraminiferal turnover across the Cenomanian–Turonian boundary (OAE2) in the northeast of the Tethys realm, Kopet-Dagh Basin. *Geologica Carpathica*, 67(5), 451–462. <https://doi.org/10.1515/geoca-2016-0028>
- Kalanat, B., Vahidinia, M., Vaziri-Moghaddam, H., Mahmudy-Gharaie, M. H., & Kumon, F. (2017). Benthic foraminiferal response to environmental changes across Cenomanian/Turonian boundary (OAE2) in the northeastern Tethys, Kopet-Dagh basin. *Journal of African Earth Sciences*, 134, 33–47. <https://doi.org/10.1016/j.jafrearsci.2017.05.019>
- Keller, G., Adatte, T., Berner, Z., Chellai, E. H., & Stüben, D. (2008). Oceanic events and biotic effects of the Cenomanian–Turonian anoxic event, Tarfaya Basin, Morocco. *Cretaceous Research*, 29(5–6), 976–994. <https://doi.org/10.1016/j.cretres.2008.05.020>
- Keller, G., & Pardo, A. (2004). Age and paleoenvironment of the Cenomanian–Turonian global stratotype section and point at Pueblo, Colorado. *Marine Micropaleontology*, 51(1–2), 95–128. <https://doi.org/10.1016/j.marmicro.2003.08.004>

- Kelley, K. A., Plank, T., Ludden, J., & Staudigel, H. (2003). Composition of altered oceanic crust at ODP Sites 801 and 1149. *Geochemistry, Geophysics, Geosystems*, 4(6), 8910. <https://doi.org/10.1029/2002gc000435>
- Kingsbury, C. G., Kamo, S. L., Ernst, R. E., Söderlund, U., & Cousins, B. L. (2018). U-Pb geochronology of the plumbing system associated with the Late Cretaceous Strand Fiord Formation, Axel Heiberg Island, Canada: Part of the 130–90 Ma High Arctic large igneous province. *Journal of Geodynamics*, 118, 106–117. <https://doi.org/10.1016/j.jog.2017.11.001>
- Kolonic, S., Wagner, T., Forster, A., Sinninghe Damsté, J. S., Walsworth-Bell, B., Erba, E., et al. (2005). Black shale deposition on the northwest African shelf during the Cenomanian/Turonian oceanic anoxic event: Climate coupling and global organic carbon burial. *Paleoceanography*, 20(1), PA1006. <https://doi.org/10.1029/2003pa000950>
- Košťák, M., Cech, S., Uličný, D., Sklenář, J., Ekrt, B., & Mazuch, M. (2018). Ammonites, inoceramids and stable carbon isotopes of the Cenomanian–Turonian OAE2 interval in Central Europe: Pecinov quarry, Bohemian Cretaceous Basin (Czech Republic). *Cretaceous Research*, 87, 150–173. <https://doi.org/10.1016/j.cretres.2017.04.013>
- Kuhnt, W., Holbourn, A. E., Beil, S., Aquit, M., Krawczyk, T., Flögel, S., et al. (2017). Unraveling the onset of Cretaceous Oceanic Anoxic Event 2 in an extended sediment archive from the Tarfaya-Laayoune Basin, Morocco. *Paleoceanography*, 32(8), 923–946. <https://doi.org/10.1002/2017pa003146>
- Kuroda, J., Ogawa, N., Tanimizu, M., Coffin, M., Tokuyama, H., Kitazato, H., & Ohkouchi, N. (2007). Contemporaneous massive subaerial volcanism and late cretaceous Oceanic Anoxic Event 2. *Earth and Planetary Science Letters*, 256(1–2), 211–223. <https://doi.org/10.1016/j.epsl.2007.01.027>
- Kuypers, M. M. M., Pancost, R. D., & Sinninghe Damsté, J. S. (1999). A large and abrupt fall in atmospheric CO₂ concentration during Cretaceous times. *Nature*, 399(6734), 342–345. <https://doi.org/10.1038/20659>
- Kuypers, M. M. M., Pancost, R. D., Nijenhuis, I. A., & Sinninghe Damsté, J. S. (2002). Enhanced productivity led to increased organic carbon burial in the euxinic North Atlantic basin during the late Cenomanian oceanic anoxic event. *Paleoceanography*, 17(4), 1501. <https://doi.org/10.1029/2000pa000569>
- Lamolda, M. A., Gorostidi, A., & Paul, C. R. C. (1994). Quantitative estimates of calcareous nannofossil changes across the Plenus Marls (latest Cenomanian), Dover, England: Implications for the generation of the Cenomanian–Turonian boundary event. *Cretaceous Research*, 15(2), 143–164. <https://doi.org/10.1006/cres.1994.1007>
- Laurin, J., Barclay, R. S., Sageman, B. B., Dawson, R. R., Pagani, M., Schmitz, M., et al. (2019). Terrestrial and marginal-marine record of the mid-Cretaceous Oceanic Anoxic Event 2 (OAE 2): High-resolution framework, carbon isotopes, CO₂ and sea-level change. *Paleogeography, Paleoclimatology, Paleocology*, 524, 118–136. <https://doi.org/10.1016/j.palaeo.2019.03.019>
- Leckie, R. M. (1985). Foraminifera of the Cenomanian–Turonian boundary interval, Greenhorn Formation, rock canyon anticline, Pueblo, Colorado. In L. M. Pratt, E. G. Kauffman & F. G. Zelt (Eds.), *Fine-grained deposits and biofacies of the Cretaceous Western Interior Seaway: Evidence of cyclic sedimentary processes: SEPM Field Trip Guidebook No. 4*, (pp. 139–149). <https://doi.org/10.2110/sepmfig.04.139>
- Li, X., Jenkyns, H. C., Wang, C., Hu, X., Chen, X., Wei, Y., et al. (2006). Upper Cretaceous carbon- and oxygen-isotope stratigraphy of hemipelagic carbonate facies from southern Tibet, China. *Journal of the Geological Society*, 163(2), 375–382. <https://doi.org/10.1144/0016-764905-046>
- Lu, Z., Jenkyns, H. C., & Rickaby, R. E. M. (2010). Iodine to calcium ratios in marine carbonate as a paleo-redox proxy during oceanic anoxic events. *Geology*, 38(12), 1107–1110. <https://doi.org/10.1130/g31145.1>
- MacLeod, K. G., Martin, E. E., & Blair, S. W. (2008). Nd isotopic excursion across Cretaceous ocean anoxic event 2 (Cenomanian–Turonian) in the tropical North Atlantic. *Geology*, 36(10), 811–814. <https://doi.org/10.1130/g24999a.1>
- Maher, H. D. Jr. (2001). Manifestations of the Cretaceous High Arctic large Igneous Province in Svalbard. *The Journal of Geology*, 109(1), 91–104. <https://doi.org/10.1086/317960>
- Martin, E. E., MacLeod, K. G., Jiménez Berrocoso, A., & Bourbon, E. (2012). Water mass circulation on Demerara Rise during the Late Cretaceous based on Nd isotopes. *Earth and Planetary Science Letters*, 327–328, 111–120. <https://doi.org/10.1016/j.epsl.2012.01.037>
- Monteiro, F. M., Pancost, R. D., Ridgwell, A., & Donnadieu, Y. (2012). Nutrients as the dominant control on the spread of anoxia and euxinia across the Cenomanian–Turonian oceanic anoxic event (OAE2): Model–data comparison. *Paleoceanography*, 27(4), PA4209. <https://doi.org/10.1029/2012pa002351>
- Mort, H., Jacquat, O., Adatte, T., Steinmann, P., Föllmi, K., Matera, V., et al. (2007). The Cenomanian/Turonian anoxic event at the Bonarelli level in Italy and Spain: Enhanced productivity and/or better preservation? *Cretaceous Research*, 28(4), 597–612. <https://doi.org/10.1016/j.cretres.2006.09.003>
- Navarro-Ramirez, J. P., Bodin, S., Consorti, L., & Immenhauser, A. (2017). Response of western south American epeiric-neritic ecosystem to middle Cretaceous Oceanic Anoxic Events. *Cretaceous Research*, 75, 61–80. <https://doi.org/10.1016/j.cretres.2017.03.009>
- Navarro-Ramirez, J. P., Bodin, S., & Immenhauser, A. (2016). Ongoing Cenomanian–Turonian heterozoan carbonate production in the neritic settings of Peru. *Sedimentary Geology*, 331, 78–93. <https://doi.org/10.1016/j.sedgeo.2015.10.011>
- Nederbragt, A. J., & Fiorentino, A. (1999). Stratigraphy and paleoceanography of the Cenomanian–Turonian Boundary Event in Oued Mellegue, north-western Tunisia. *Cretaceous Research*, 20(1), 47–62. <https://doi.org/10.1006/cres.1998.0136>
- Nemoto, T., & Hasegawa, T. (2011). Submillennial resolution carbon isotope stratigraphy across the Oceanic Anoxic Event 2 horizon in the Tappu section, Hokkaido, Japan. *Paleogeography, Paleoclimatology, Paleocology*, 309(3–4), 271–280. <https://doi.org/10.1016/j.palaeo.2011.06.009>
- Orth, C. J., Attrep, M., Quintana, L. R., Elder, W. P., Kauffman, E. G., Diner, R., & Villamil, T. (1993). Elemental abundance anomalies in the late Cenomanian extinction interval: A search for the source(s). *Earth and Planetary Science Letters*, 117(1–2), 189–204. [https://doi.org/10.1016/0012-821x\(93\)90126-t](https://doi.org/10.1016/0012-821x(93)90126-t)
- Ostrander, C. M., Owens, J. D., & Nielsen, S. G. (2017). Constraining the rate of oceanic deoxygenation leading up to a Cretaceous Oceanic Anoxic Event (OAE-2: ~94 Ma). *Science Advances*, 3(8), e1701020. <https://doi.org/10.1126/sciadv.1701020>
- Owens, J. D., Gill, B. C., Jenkyns, H. C., Bates, S. M., Severmann, S., Kuypers, M. M. M., et al. (2013). Sulfur isotopes track the global extent and dynamics of euxinia during Cretaceous Oceanic Anoxic Event 2. *Proceedings of the National Academy of Sciences*, 110(46), 18,407–18,412. <https://doi.org/10.1073/pnas.1305304110>
- Parente, M., Frijia, G., Di Lucia, M., Jenkyns, H. C., Woodfine, R. G., & Baroncini, F. (2008). Stepwise extinction of larger foraminifers at the Cenomanian–Turonian boundary: A shallow-water perspective on nutrient fluctuations during Oceanic Anoxic Event 2 (Bonarelli Event). *Geology*, 36(9), 715–718. <https://doi.org/10.1130/g24893a.1>
- Paul, C. R. C., Lamolda, M. A., Mitchell, S. F., Vaziri, M. R., Gorostidi, A., & Marshall, J. D. (1999). The Cenomanian–Turonian boundary at Eastbourne (Sussex, UK): A proposed European reference section. *Paleogeography, Paleoclimatology, Paleocology*, 150(1–2), 83–121. [https://doi.org/10.1016/s0031-0182\(99\)00009-7](https://doi.org/10.1016/s0031-0182(99)00009-7)

- Pearce, M. A., Jarvis, I., & Tocher, B. A. (2009). The Cenomanian–Turonian boundary event, OAE2 and paleoenvironmental change in epicontinental seas: New insights from the dinocyst and geochemical records. *Paleogeography, Paleoclimatology, Paleoecology*, *280*(1–2), 207–234. <https://doi.org/10.1016/j.paleo.2009.06.012>
- Pedersen, T. F., & Calvert, S. E. (1990). Anoxia vs. productivity: What controls the formation of organic-carbon-rich sediments and sedimentary rocks? *AAPG Bulletin*, *74*(4), 454–466. <https://doi.org/10.1306/0c9b232b-1710-11d7-8645000102c1865d>
- Peryt, D., & Lamolda, M. (1996). Benthonic foraminiferal mass extinction and survival assemblages from the Cenomanian–Turonian Boundary Event in the Menoyo Section, northern Spain. *Geological Society, London, Special Publications*, *102*(1), 245–258. <https://doi.org/10.1144/gsl.sp.1996.001.01.18>
- Pin, C., & Zalduegui, J. S. (1997). Sequential separation of light rare-earth elements, thorium and uranium by miniaturized extraction chromatography: Application to isotopic analyses of silicate rocks. *Analytica Chimica Acta*, *339*(1–2), 79–89. [https://doi.org/10.1016/s0003-2670\(96\)00499-0](https://doi.org/10.1016/s0003-2670(96)00499-0)
- Pogge von Strandmann, P. A. E., Jenkyns, H. C., & Woodfine, R. G. (2013). Lithium isotope evidence for enhanced weathering during Oceanic Anoxic Event 2. *Nature Geoscience*, *6*(8), 668–672. <https://doi.org/10.1038/ngeo1875>
- Pratt, L. M. (1985). Isotopic studies of organic matter and carbonate in rocks of the Greenhorn Marine Cycle. In L. M. Pratt, E. G. Kauffman, & F. B. Zelt (Eds.), *Fine-grained deposits and biofacies of the Cretaceous Western Interior Seaway: Evidence of cyclic sedimentary processes, SEPM Field Trip Guidebook* (Vol. 4, pp. 38–48). <https://doi.org/10.2110/sepmfg.04>
- Prokoph, A., Babalola, L. O., El Bilali, H., Olagoke, S., & Rachold, V. (2013). Cenomanian–Turonian carbon isotope stratigraphy of the Western Canadian Sedimentary Basin. *Cretaceous Research*, *44*, 39–53. <https://doi.org/10.1016/j.cretres.2013.03.005>
- Remmelzwaal, S. R., Sadekov, A. Y., Parkinson, I. J., Schmidt, D. N., Titelboim, D., Abramovich, S., ... Kimoto, K. (2019). Post-depositional overprinting of chromium in foraminifera. *Earth and Planetary Science Letters*, *515*, 100–111. <https://doi.org/10.1016/j.epsl.2019.03.001>
- Robinson, S. A., Dickson, A. J., Pain, A., Jenkyns, H. C., O'Brien, C. L., Farnsworth, A., & Lunt, D. J. (2019). Southern Hemisphere sea-surface temperatures during the Cenomanian–Turonian: Implications for the termination of Oceanic Anoxic Event 2. *Geology*, *47*(2), 131–134. <https://doi.org/10.1130/g45842.1>
- Rudnick, R. L., & Gao, S. (2003). Composition of the continental crust. *Treatise on Geochemistry*, *3*, 659. <https://doi.org/10.1016/B0-08-043751-6/03016-4>
- Sageman, B. B., Meyers, S. R., & Arthur, M. A. (2006). Orbital time scale and new C-isotope record for Cenomanian–Turonian boundary stratotype. *Geology*, *34*(2), 125. <https://doi.org/10.1130/g22074.1>
- Scaife, J. D., Ruhl, M., Dickson, A. J., Mather, T. A., Jenkyns, H. C., Percival, L. M. E., et al. (2017). Sedimentary Mercury Enrichments as a Marker for Submarine Large Igneous Province Volcanism? Evidence from the Mid-Cenomanian Event and Oceanic Anoxic Event 2 (Late Cretaceous). *Geochemistry, Geophysics, Geosystems*, *18*(12), 4253–4275. <https://doi.org/10.1002/2017gc007153>
- Schlanger, S. O., Arthur, M. A., Jenkyns, H. C., & Scholle, P. A. (1987). The Cenomanian–Turonian Oceanic Anoxic Event, I. stratigraphy and distribution of organic carbon-rich beds and the marine $\delta^{13}\text{C}$ excursion. *Geological Society, London, Special Publications*, *26*(1), 371–399. <https://doi.org/10.1144/gsl.sp.1987.026.01.24>
- Schlanger, S. O., & Jenkyns, H. C. (1976). Cretaceous oceanic anoxic events: Causes and consequences. *Geologie en Mijnbouw*, *55*(3–4).
- Scholle, P. A. (1974). Diagenesis of Upper Cretaceous chalks from England, Northern Ireland and the North Sea. In K. J. Hsü & H. C. Jenkyns (Eds.), *Pelagic Sediments: On Land and Under the Sea*, *1*, 177–210, Special Publications International Association of Sediementologists. <https://doi.org/10.1002/9781444304855.ch8>
- Scholle, P. A., & Arthur, M. A. (1980). Carbon isotope fluctuations in cretaceous pelagic limestones: Potential stratigraphic and petroleum exploration tool. *AAPG Bulletin*, *60*(1), 67–87. <https://doi.org/10.1306/2f91892d-16ce-11d7-8645000102c1865d>
- Schröder-Adams, C. J., Herrle, J. O., Selby, D., Quesnel, A., & Froude, G. (2019). Influence of the High Arctic Igneous Province on the Cenomanian/Turonian boundary interval, Sverdrup Basin, High Canadian Arctic. *Earth and Planetary Science Letters*, *511*, 76–88. <https://doi.org/10.1016/j.epsl.2019.01.023>
- Scotese, C. R. (2014). Atlas of Late Cretaceous paleogeographic maps, PALEOMAP atlas for ArcGIS, volume 2, The Cretaceous, Maps 16–22, Mollweide Projection. *ResearchGate Academia*. <https://doi.org/10.13140/2.1.4099.4560>
- Sinninghe Damsté, J. S., Kuypers, M. M. M., Pancost, R. D., & Schouten, S. (2008). The carbon isotopic response of algae, (cyano)bacteria, archaea and higher plants to the late Cenomanian perturbation of the global carbon cycle: Insights from biomarkers in black shales from the Cape Verde Basin (DSDP Site 367). *Organic Geochemistry*, *39*(12), 1703–1718. <https://doi.org/10.1016/j.orggeochem.2008.01.012>
- Sinninghe Damsté, J. S., van Bentum, E. C., Reichart, G.-J., Pross, J., & Schouten, S. (2010). A CO₂ decrease-driven cooling and increased latitudinal temperature gradient during the mid-Cretaceous Oceanic Anoxic Event 2. *Earth and Planetary Science Letters*, *293*(1–2), 97–103. <https://doi.org/10.1016/j.epsl.2010.02.027>
- Snow, L. J., Duncan, R. A., & Bralower, T. J. (2005). Trace element abundances in the Rock Canyon Anticline, Pueblo, Colorado, marine sedimentary section and their relationship to Caribbean plateau construction and oxygen anoxic event 2. *Paleoceanography*, *20*(3), PA3005. <https://doi.org/10.1029/2004pa001093>
- Sweere, T. C., Dickson, A. J., Jenkyns, H. C., Porcelli, D., Elrick, M., van den Boorn, S. H. J. M., & Henderson, G. M. (2018). Isotopic evidence for changes in the zinc cycle during Oceanic Anoxic Event 2 (Late Cretaceous). *Geology*, *46*(5), 463–466. <https://doi.org/10.1130/g40226.1>
- Takashima, R., Nishi, H., Hayashi, K., Okada, H., Kawahata, H., Yamanaka, T., et al. (2009). Litho-, bio- and chemostratigraphy across the Cenomanian/Turonian boundary (OAE 2) in the Vocontian Basin of southeastern France. *Paleogeography, Paleoclimatology, Paleoecology*, *273*(1–2), 61–74. <https://doi.org/10.1016/j.palaeo.2008.12.001>
- Tanaka, T., Togashi, S., Kamioka, H., Amakawa, H., Kagami, H., Hamamoto, T., et al. (2000). JNd-1: A neodymium isotopic reference in consistency with La Jolla neodymium. *Chemical Geology*, *168*(3–4), 279–281. [https://doi.org/10.1016/s0009-2541\(00\)00198-4](https://doi.org/10.1016/s0009-2541(00)00198-4)
- Taylor, S. R., & McLennan, S. M. (1995). The geochemical evolution of the continental crust. *Reviews of Geophysics*, *33*(2), 241. <https://doi.org/10.1029/95rg00262>
- Tegner, C., Storey, M., Holm, P. M., Thorarinnsson, S. B., Zhao, X., Lo, C.-H., & Knudsen, M. F. (2011). Magmatism and Eureka deformation in the High Arctic Large Igneous Province: ⁴⁰Ar–³⁹Ar age of Kap Washington Group volcanics, North Greenland. *Earth and Planetary Science Letters*, *303*(3–4), 203–214. <https://doi.org/10.1016/j.epsl.2010.12.047>
- Thomas, D. J. (2005). Reconstructing ancient deep-sea circulation patterns using the Nd isotopic composition of fossil fish debris. *Isotopic and Elemental Tracers of Cenozoic Climate Change*, *395*, 1. <https://doi.org/10.1130/0-8137-2395-7.1>
- Thomas, D. J., & Tilghman, D. S. (2014). Geographically different oceanographic responses to global warming during the Cenomanian–Turonian interval and Oceanic Anoxic Event 2. *Paleogeography, Paleoclimatology, Paleoecology*, *411*, 136–143. <https://doi.org/10.1016/j.paleo.2014.06.014>

- Tostevin, R., Shields, G. A., Tarbuck, G. M., He, T., Clarkson, M. O., & Wood, R. A. (2016). Effective use of cerium anomalies as a redox proxy in carbonate-dominated marine settings. *Chemical Geology*, *438*, 146–162. <https://doi.org/10.1016/j.chemgeo.2016.06.027>
- Trabucho-Alexandre, J. (2014). More gaps than shale: Erosion of mud and its effect on preserved geochemical and paleobiological signals. *Geological Society, London, Special Publications*, *404*(1), 251–270. <https://doi.org/10.1144/sp404.10>
- Tsikos, H., Jenkyns, H. C., Walsworth-Bell, B., Petrizzo, M. R., Forster, A., Kolonic, S., et al. (2004). Carbon-isotope stratigraphy recorded by the Cenomanian–Turonian Oceanic Anoxic Event: Correlation and implications based on three key localities. *Journal of the Geological Society*, *161*(4), 711–719. <https://doi.org/10.1144/0016-764903-077>
- Turgeon, S. C., & Creaser, R. A. (2008). Cretaceous oceanic anoxic event 2 triggered by a massive magmatic episode. *Nature*, *454*(7202), 323–326. <https://doi.org/10.1038/nature07076>
- Van Bentum, E. C., Reichert, G.-J., Forster, A., & Sinninghe Damsté, J. S. (2012). Latitudinal differences in the amplitude of the OAE-2 carbon isotopic excursion: $p\text{CO}_2$ and paleo productivity. *Biogeosciences*, *9*(2), 717–731. <https://doi.org/10.5194/bg-9-717-2012>
- van Helmond, N. A. G. M., Ruvalcaba Baroni, I., Sluijs, A., Sinninghe Damsté, J. S., & Slomp, C. P. (2014). Spatial extent and degree of oxygen depletion in the deep proto-North Atlantic basin during Oceanic Anoxic Event 2. *Geochemistry, Geophysics, Geosystems*, *15*, 4254–4266. <https://doi.org/10.1002/2014GC005528>
- Van Helmond, N. A. G. M., Sluijs, A., Papadomanolaki, N. M., Plint, A. G., Gröcke, D. R., Pearce, M. A., et al. (2016). Equatorward phytoplankton migration during a cold spell within the Late Cretaceous super-greenhouse. *Biogeosciences*, *13*(9), 2859–2872. <https://doi.org/10.5194/bg-13-2859-2016>
- Van Helmond, N. A. G. M., Sluijs, A., Reichert, G.-J., Sinninghe Damsté, J. S., Slomp, C. P., & Brinkhuis, H. (2013). A perturbed hydrological cycle during Oceanic Anoxic Event 2. *Geology*, *42*(2), 123–126. <https://doi.org/10.1130/g34929.1>
- van Helmond, N. A. G. M., Sluijs, A., Sinninghe Damsté, J. S., Reichert, G.-J., Voigt, S., Erbacher, J., et al. (2015). Freshwater discharge controlled deposition of Cenomanian–Turonian black shales on the NW European epicontinental shelf (Wunstorf, northern Germany). *Climate of the Past*, *11*(3), 495–508. <https://doi.org/10.5194/cp-11-495-2015>
- van Hinsbergen, D. J. J., de Groot, L. V., van Schaik, S. J., Spakman, W., Bijl, P. K., Sluijs, A., et al. (2015). A paleolatitude calculator for paleoclimate studies. *PLoS ONE*, *10*(6), e0126946. <https://doi.org/10.1371/journal.pone.0126946>
- Voigt, S. (2000). Cenomanian–Turonian composite $\delta^{13}\text{C}$ curve for Western and Central Europe: The role of organic and inorganic carbon fluxes. *Paleogeography, Paleoclimatology, Paleoecology*, *160*(1–2), 91–104. [https://doi.org/10.1016/s0031-0182\(00\)00060-2](https://doi.org/10.1016/s0031-0182(00)00060-2)
- Voigt, S., Aurag, A., Leis, F., & Kaplan, U. (2007). Late Cenomanian to Middle Turonian high-resolution carbon isotope stratigraphy: New data from the Münsterland Cretaceous Basin, Germany. *Earth and Planetary Science Letters*, *253*(1–2), 196–210. <https://doi.org/10.1016/j.epsl.2006.10.026>
- Voigt, S., Erbacher, J., Mutterlose, J., Weiss, W., Westerhold, T., Wiese, F., et al. (2008). The Cenomanian–Turonian of the Wunstorf section (North Germany): Global stratigraphic reference section and new orbital time scale for Oceanic Anoxic Event 2. *Newsletters on Stratigraphy*, *43*(1), 65–89. <https://doi.org/10.1127/0078-0421/2008/0043-0065>
- Voigt, S., Gale, A. S., & Flögel, S. (2004). Midlatitude shelf seas in the Cenomanian–Turonian greenhouse world: Temperature evolution and North Atlantic circulation. *Paleoceanography*, *19*, PA4020. <https://doi.org/10.1029/2004PA001015>
- Voigt, S., Gale, A. S., & Voigt, T. (2006). Sea-level change, carbon cycling and palaeoclimate during the Late Cenomanian of Northwest Europe; an integrated palaeoenvironmental analysis. *Cretaceous Research*, *27*(6), 836–858. <https://doi.org/10.1016/j.cretres.2006.04.005>
- Voigt, S., & Hilbrecht, H. (1997). Late Cretaceous carbon isotope stratigraphy in Europe: correlation and relations with sea level and sediment stability. *Palaeogeography, Palaeoclimatology, Paleoecology*, *134*(1–4), 39–59. [https://doi.org/10.1016/s0031-0182\(96\)00156-3](https://doi.org/10.1016/s0031-0182(96)00156-3)
- Voigt, S., & Wiese, F. (2000). Evidence for Late Cretaceous (Late Turonian) climate cooling from oxygen-isotope variations and palaeobiogeographic changes in Western and Central Europe. *Journal of the Geological Society*, *157*(4), 737–743. <https://doi.org/10.1144/jgs.157.4.737>
- Webb, G. E., & Kamber, B. S. (2000). Rare earth elements in Holocene reefal microbialites: A new shallow seawater proxy. *Geochimica et Cosmochimica Acta*, *64*(9), 1557–1565. [https://doi.org/10.1016/S0016-7037\(99\)00400-7](https://doi.org/10.1016/S0016-7037(99)00400-7)
- Wendler, I. (2013). A critical evaluation of carbon isotope stratigraphy and biostratigraphic implications for Late Cretaceous global correlation. *Earth-Science Reviews*, *126*, 116–146. <https://doi.org/10.1016/j.earscirev.2013.08.003>
- Wendler, J. E., Wendler, I., Vogt, C., & Kuss, J. (2016). Link between cyclic eustatic sea-level change and continental weathering: Evidence for aquifer-eustasy in the Cretaceous. *Paleogeography, Paleoclimatology, Paleoecology*, *441*, 430–437. <https://doi.org/10.1016/j.paleo.2015.08.014>
- Zaghib-Turki, D., & Soua, M. (2013). High resolution biostratigraphy of the Cenomanian–Turonian interval (OAE2) based on planktonic foraminiferal bioevents in north-central Tunisia. *Journal of African Earth Sciences*, *78*, 97–108. <https://doi.org/10.1016/j.jafrearsci.2012.09.014>
- Zheng, X.-Y., Jenkyns, H. C., Gale, A. S., Ward, D. J., & Henderson, G. M. (2013). Changing ocean circulation and hydrothermal inputs during Ocean Anoxic Event 2 (Cenomanian–Turonian): Evidence from Nd-isotopes in the European shelf sea. *Earth and Planetary Science Letters*, *375*, 338–348. <https://doi.org/10.1016/j.epsl.2013.05.053>
- Zheng, X.-Y., Jenkyns, H. C., Gale, A. S., Ward, D. J., & Henderson, G. M. (2016). A climatic control on reorganization of ocean circulation during the mid-Cenomanian event and Cenomanian–Turonian oceanic anoxic event (OAE 2): Nd isotope evidence. *Geology*, *44*(2), 151–154. <https://doi.org/10.1130/g37354.1>
- Zhou, X., Jenkyns, H. C., Owens, J. D., Junium, C. K., Zheng, X.-Y., Sageman, B. B., et al. (2015). Upper Ocean oxygenation dynamics from I/Ca ratios during the Cenomanian–Turonian OAE 2. *Paleoceanography*, *30*(5), 510–526. <https://doi.org/10.1002/2014pa002741>